ROLE OF SPONTANEOUS DNA DAMAGE AND SINGLE-STRANDED DNA IN GENERATION OF ENLARGED G_2 PHASE CELLS IN *RAD52* MUTANTS OF *SACCHAROMYCES CEREVISIAE*

By

Corbin J. England, B.S.

A thesis submitted to the Graduate Council of
Texas State University in partial fulfillment
of the requirements for the degree of
Master of Science
with a Major in Biochemistry
December 2018

Committee Members:

L. Kevin Lewis, Chair

Liqin Du

Wendi David

FAIR USE AND AUTHOR'S PERMISSION STATEMENT

Fair Use

Duplication Permission

ACKNOWLEDGEMENTS

The superhuman levels of dedication and attention Dr. Kevin Lewis gave to me and my project, an open-door policy that lasted from sunup to sundown, a willingness to answer questions no matter how tangential, and working overtime to help me prepare my thesis made all this possible. Dr. Lewis, you have been an amazing advisor and I cannot thank you enough for all your help and hard work.

Thank you to Dr. Holland, who was always available to answer questions whenever Dr. Lewis wasn't.

Thank you to all the past and present members of the Kevin Lewis lab who helped to make my time here so enjoyable. Monica, Angelica, and Shuba, you are the three funniest women I have ever met. Nestor, you are one of the closest friends I've had for a long while. Alex, you're a great guy and I'm sorry for any jokes that went too far. Sarah, it was always a nice surprise to see you when I was working during evenings and nights. A great big thank you goes out to everyone else in the lab and my friends in other labs.

To my parents, thank you. A million times thank you. Knowing that you were never more than a phone call or a couple hours' drive away means more than I know how to express. Dad, the blessing of two debt-free degrees is so massive I'm sure it will be years before I can completely comprehend it. Mom, you were always there for me when I needed to vent or ask if these leftovers were still good. Thank you.

TABLE OF CONTENTS

Page

LIST OF TABLES

Table **Page**

LIST OF FIGURES

Figure **Page**

I. INTRODUCTION

Deoxyribonucleic acid (DNA) is a polymeric biomolecule found in all known forms of life. The monomers of DNA are linked by phosphodiester bonding between the phosphate group and deoxyribose sugar of individual nucleotides. DNA is given its characteristic double helical shape by single strands of DNA bonding via their bases. These strands run in opposite direction to each other, one in the 3' to 5' direction and the other in the 5' to 3' direction. Of the four bases, cytosine forms hydrogen bonds with guanine and adenine forms hydrogen bonds with thymine. Alteration of the base sequence in genes because of damage to the DNA can alter the gene products, and is capable of adversely affecting living systems (1-2).

Different pathways of DNA repair exist that are capable of responding to different types of DNA damage (1). Damage to DNA can arise from a variety of both endogenous and exogenous sources (3-5). Sources of endogenous damage include reactive oxygen species (ROS), stalled replication forks, and certain metabolic processes (1-4, 6). Sources of exogenous DNA damage include ultraviolet and ionizing radiation as well as chemical mutagens such as bleomycin, methyl methanesulfonate, and nitrosamines (1, 7-8). DNA damage events occur in humans at a frequency of 50,000 to 100,000 times per cell every day (2-3). Any unrepaired or misrepaired lesions can be harmful to living beings, potentially causing mutations leading to dysfunctional cells and/or cancer. For example, genetic diseases such as Werner's and Bloom's Syndrome are caused by defects in DNA repair and are characterized by high incidences of cancer (9-10).

Types of DNA damage

The causes and types of DNA damage are many and diverse (1-2). ROS such as hydroxyl radicals or superoxide radicals can cause oxidative damage to DNA (11). This frequently involves the creation of a modified base such as 8-hydroxyguanine, but can also involve damage to the deoxyribose sugar and the phosphate (12). Another type of base damage is deamination, where a base's amine group can be removed (13). One example of this is the transformation of cytosine to uracil, a base normally only found in ribonucleic acid (RNA) (13). The purine bases in DNA can be lost by depurination caused by chemicals such as aromatic hydrocarbons (14). Ultraviolet (UV) light can cause pyrimidines, cytosine and thymine, to covalently link with each other if they are adjacent on either the same strand or opposite strands. These crosslinks, if not repaired, can interfere with DNA replication and transcription, which can lead to the death of the cell (3, 15). Ionizing radiation and chemicals such as bleomycin can cause single-stranded and double-stranded breaks (SSBs and DSBs) (1, 7-8). DSBs can be considered the most dangerous form of DNA damage, as even a single DSB can be lethal to a cell (16-17). If the repair process goes awry mutations could occur, the genome could be rearranged, or an entire chromosome could be lost (17).

Modes of DNA damage repair

DNA lesions are repaired through specialized pathways rather than a single general process (Figure 1). These repair processes make use of a variety of different enzymes, such as polymerases, phosphatases, isomerases, helicases, nucleases, ligases, recombinases, kinases, and more (1, 8, 18). Base excision repair (BER) removes

damaged bases and replaces them with undamaged ones (3, 19). Nucleotide excision repair (NER) is used to remove and repair bulky adducts in DNA, as well as crosslinked nucleotides and nearby bases before replacing them with new ones (20). DSBs can be repaired by either nonhomologous end-joining (NHEJ) or homologous recombination (HR) (21-25). NHEJ repairs DSBs by joining them directly, without the use of an unbroken DNA template (21-23). HR resections the ends of a DSB to generate long strands of single-stranded DNA (ssDNA) (24-25). The ssDNA strands will then invade a homologous sequence of dsDNA, such as on a sister chromatid, and use that as a template for repair. Due to this feature, HR normally involves little to no loss of genetic information (24-25).

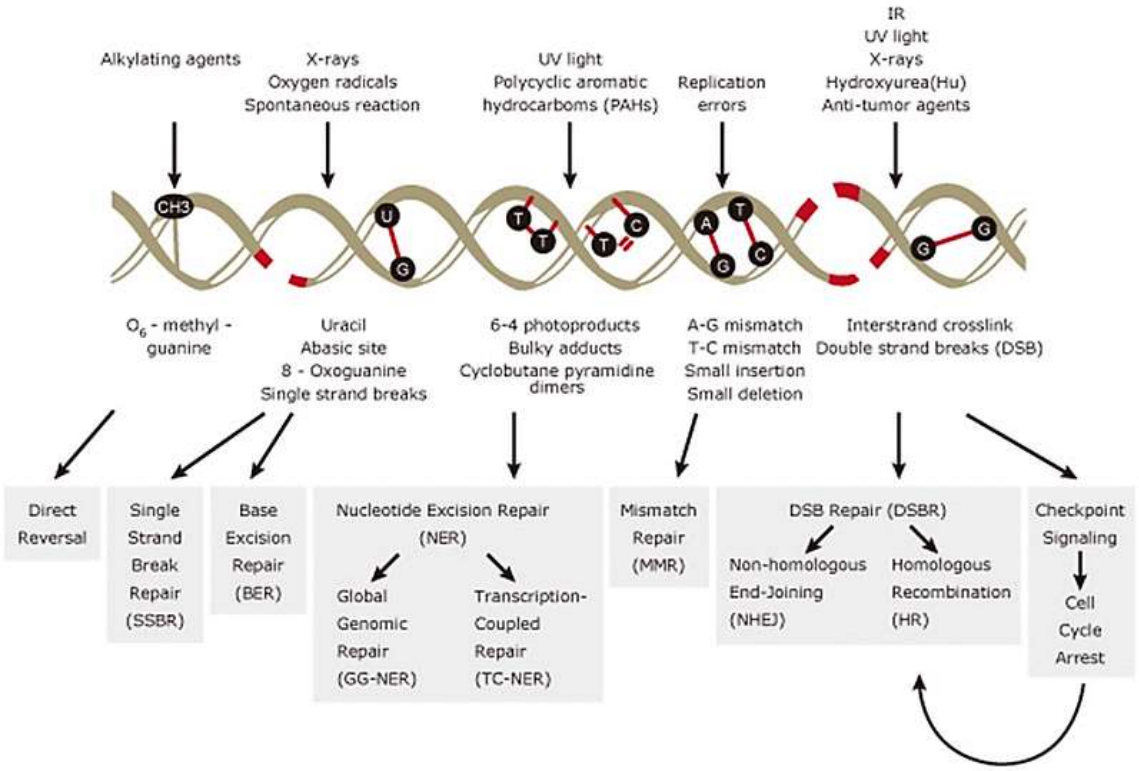

Figure 1. Types of DNA damage and their repair pathways. Five different general sources of DNA damage and eight different methods of repair are shown. Each type of damage has at least one method of repair dedicated solely to that damage, rather than a general repair method for all types of damage. Image taken from http://www.bio-connect.nl.

Repair of DSBs via HR

Homologous recombination is the primary method of repairing DSBs in the budding yeast *Saccharomyces cerevisiae* (24-26). HR is less prone to mutation than NHEJ since it makes use of a homologous sequence of DNA to guide the repair of the DSB. The Rad52 protein family, which includes Rad50, Rad51, Rad52, Rad54, Rad55, Rad57, Rad59, Xrs2, Rdh54, and Mre11, plays a vital role in HR (24-25, 27). The first

step of HR involves the Mrx complex, composed of Mre11, Rad50, and Xrs2, along with Sae2, which carry out a short resectioning of the 5' ends of the DSB and generate short 3' tails of ssDNA that are 50 to 100 nucleotides long (5, 28-30). In the second step, Exo1 and the Sgs1-Dna2 helicase-nuclease complex carry out further resectioning to generate longer 3' tails. The topoisomerase Top3 and Rmi1 may also play a role in the second step of resection (30-32). During the third step, the ssDNA binding protein complex Rpa, composed of Rfa1, Rfa2, and Rfa3, binds to the long 3' tails (30, 33) (Figure2). This is thought to act as a signal for the recruitment of DNA damage checkpoint response proteins, which can halt the cell in G_2 phase of the cell cycle (5, 8, 33). The DNA damage checkpoint is mediated by Mec1, Mec3, Rad9, Rad17, and several other proteins (5, 8, 34). During these processes, nucleosome remodeling is occurring thanks to the Rsc complex, and sister chromatid cohesion is being carried out by proteins such as Eco1, Scc2, Smc5, and Smc6 (24-25, 28). After the resected ssDNA ends are bound by Rpa, the Rad51 and Rad52 proteins and other members of the Rad52 group bind to the 3' tails and begin seeking out a homologous sequence of dsDNA (24-25, 27). Once a homologous sequence is found, a long 3' tail invades the unbroken duplex and DNA replication begins. This is followed by processes such as branch migration, resolution, ligation, and nucleosome reassembly, and eventually results in a repaired DSB. A simplified flow diagram depicting the process of HR in yeast cells can be seen in Figure 2.

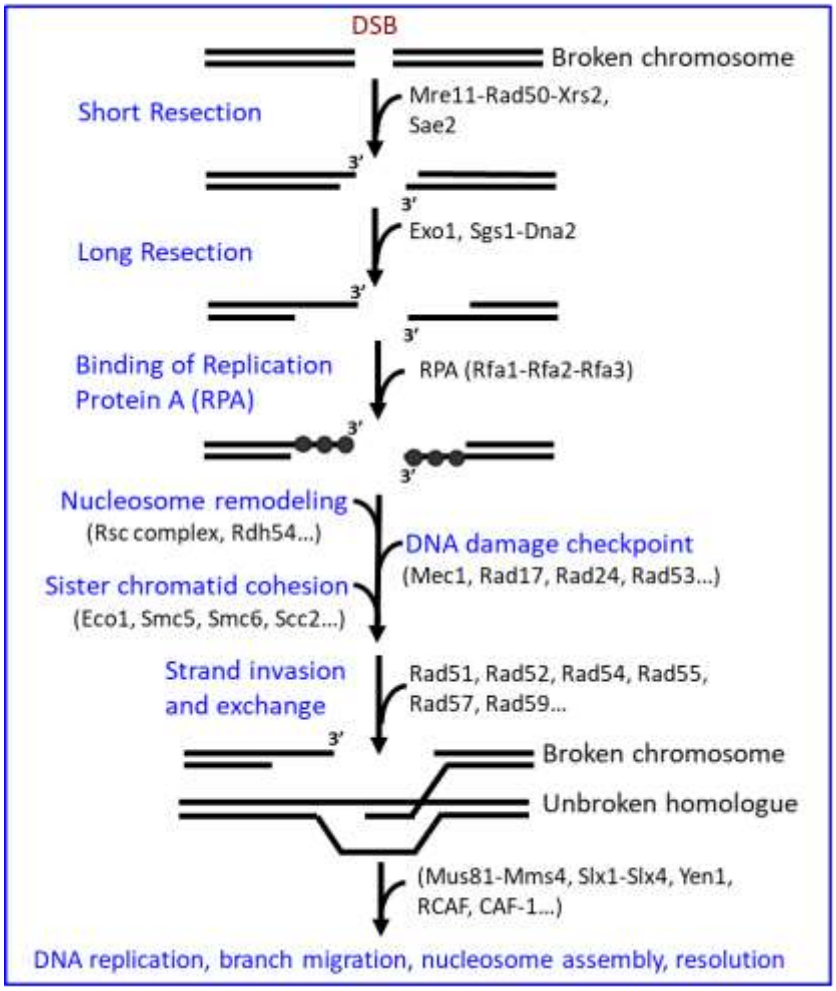

Figure 2. Homologous recombination in *Saccharomyces cerevisiae*. A short resection and then long resection of the ends of the DSB takes place before the binding of Rpa. Members of the Rad52 protein group facilitate the strand invasion and exchange with a homologous segment of dsDNA (24-25, 28).

During HR, multiple DSBs gather together for repair in nuclear locations with high concentrations of Rad52, known as Rad52 foci (16, 35). This was discovered by engineering *S. cerevisiae* cells to contain segments of DNA where DSBs could be induced that were surrounded by binding sites for LacI repressor protein. These cells were also made to produce fully functional fusions of Rad52 with cyan fluorescent protein (CFP) and LacI with yellow fluorescent protein (YFP). When the DSBs were

induced, 94% of all Rad52::CFP foci were observed to be colocalized with the LacI::YFP foci, whereas yeast cells lacking the inducible DSB site rarely displayed colocalization of the two protein fusions (16). Spontaneously occurring foci were most often observed in S phase cells, suggesting that some DSBs occurred during normal cell growth and were associated with DNA replication (35).

DNA damage checkpoint response

As seen in Figure 3, growing eukaryotic cells pass through four phases: gap phase 1 (G_1), S phase, gap phase 2 (G_2), and mitosis (M) phase (5). During G_1 phase the cells are growing and accumulating everything they will need to enter S phase. While in S phase the cell is replicating all of its DNA to create sister chromatids. During G_2 phase the cell continues growing and prepares itself to enter M phase. During M phase the sister chromatids are aligned by the mitotic spindle and then split so that each daughter cell gets one complete copy of every chromosome. During this process other important organelles are also divided as the cell divides. Passage through the cell cycle is known to be associated with an increase in the sizes of yeast cells during progression from G_1 to S to G_2 phase (36). While growing, if the cell detects damage to its DNA, it is capable of pausing in G_2 phase (5). Although this is called the G_2 DNA damage checkpoint, in *S. cerevisiae* cell cycling actually halts between metaphase and anaphase thanks to the transition from G_2 to M phase being poorly defined in this species (5). In addition, *S. cerevisiae* cells are also capable of pausing in response to DNA damage during the transition from G_1 to S phase and during S phase. G_2 pausing is dominant in response to DNA damage and, as seen in Figure 4, is characterized by an increased percentage of G_2 cells in *S. cerevisiae* cultures after exposure to DNA damaging agents.

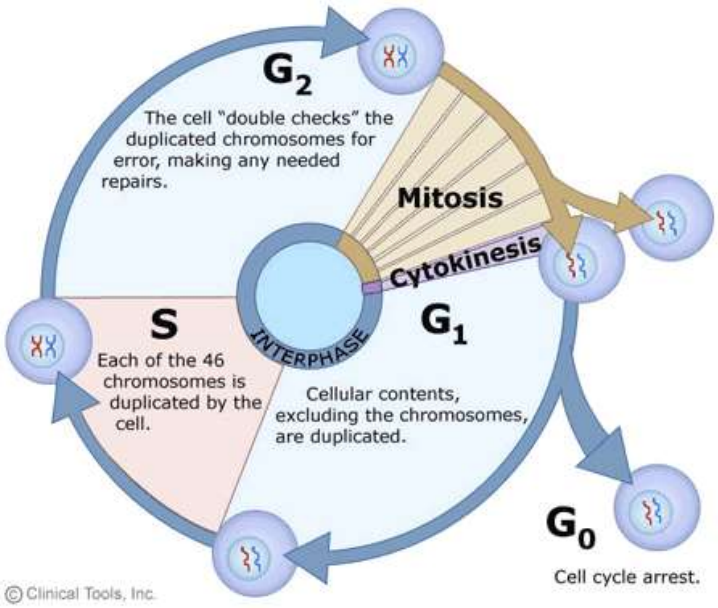

Figure 3. The four phases of the cell cycle. During G_1 phase the cell grows and prepares to enter S phase. During S phase the cell duplicates its chromosomes. During G_2 phase the cell arranges itself for division. During M phase the cell's chromosomes are segregated via the mitotic spindle and the cell splits into two daughter cells. Image taken from https://www2.le.ac.uk

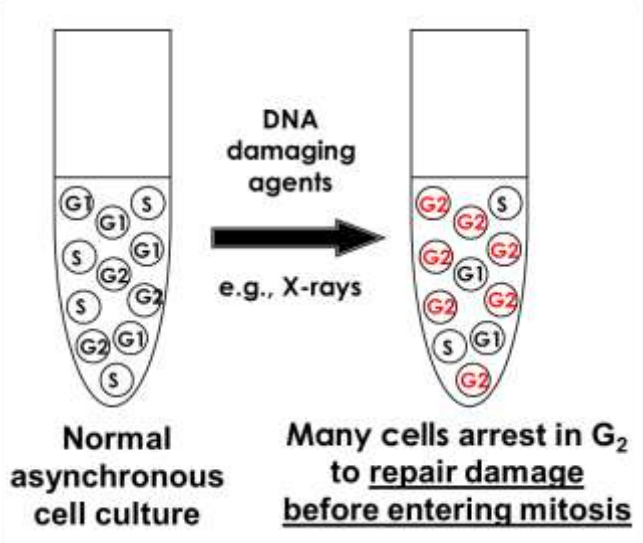

Figure 4. Cells growing in culture contain a mixture of G_1, S, G_2, and M phase cells. After exposure to DNA damaging agents such as X-rays, cells pause in G_2. This increases the amount of G_2 phase cells in the culture.

Properties of the model organism *Saccharomyces cerevisiae*

S. cerevisiae is a budding yeast, and as such its progress through the cell cycle can be followed by the use of light microscopy (Figure 5A). Unbudded cells are in G_1 phase, cells with buds less than 50% of the size of the mother cell are in S phase, and cells with buds equal to or larger than 50% of the size of the mother cell are in either G_2 or M phase (Figure 5B) (34, 37). These yeast cells are capable of living and growing in either a haploid or diploid state. They possess two mating types, mating type a (*MATa*) and mating type alpha (*MATα*), and interactions between these two types can lead to fusion and formation of a/α diploid cells (38). Many of the proteins *S. cerevisiae* cells use to repair DSBs have homologues in human cells (28, 35). This observation, combined with their short doubling time and economical nature, make them a useful model for the study of DNA repair.

a

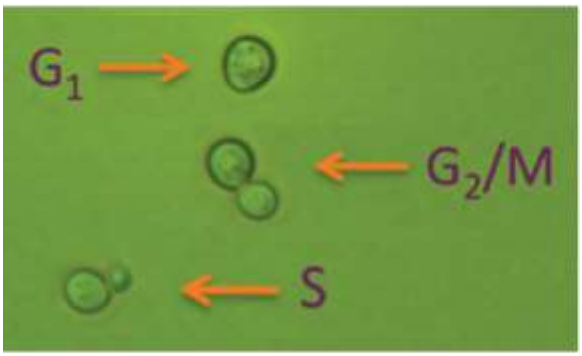

b

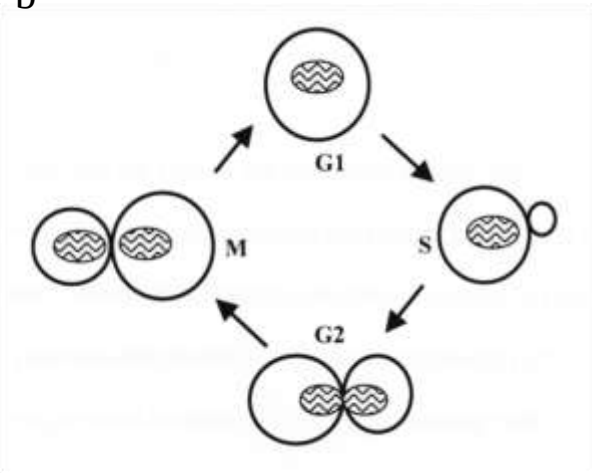

Figure 5. Classification of bud size and *S. cerevisiae* cells' passage through the cell cycle. a) Phase contrast images of *S. cerevisiae* cells as unbudded, small-budded, and large-budded cells. b) A representation of the bud size and nucleus position during the cell cycle in *S. cerevisiae*.

Unusual characteristics of *rad52* cells

rad52 deletion mutants of *S. cerevisiae* have a number of interesting properties. The suffix *rad* comes from the fact that yeast cells lacking this gene are sensitive to ionizing radiation (27-28). In addition, *rad52* mutants are sensitive to bleomycin and other chemicals that cause DSBs. This is because, without the Rad52 protein, yeast cells are unable to effectively carry out HR, which is the main method of DSB repair. Genetic exchange between sister chromatids is a vital step in meiosis (39). Rad52 plays an important role in this process and as such *rad52* cells also display lower levels of meiotic recombination (39). It has been demonstrated that *rad52* cells have slower doubling times than WT cells (9). Recently, the phosphorylation of Rad52 has been linked to regulation of the spindle assembly checkpoint, revealing a potential new function for the protein (40).

ROS and antioxidants

ROS are both useful and harmful to eukaryotic cells. Phagocytes engulf invasive foreign cells and then use a cocktail that includes, among other molecules, ROS such as hydrogen peroxide and superoxide radicals to destroy them (41). Such free radicals loose inside an average eukaryotic cell can damage not only DNA and RNA, but also proteins and lipids (11, 42). Metals such as lead and iron can be one source of radicals inside a living system, and metal chelating proteins can serve as antioxidants by sequestering them (42). Antioxidants are defined as any molecule that reduces the rate of oxidation or outright prevents it (42). The ability of *S. cerevisiae* cells to grow in the presence or absence of oxygen allow its role as a model eukaryotic organism to be extended to cover the study of antioxidants (43).

Previous work in the lab

Previous work by graduate student Monica Weis demonstrated that liquid cultures of *S. cerevisiae rad52* mutants contain higher percentages of large-budded cells than WT cell cultures during normal growth. In order to determine whether these large-budded cells were in G_2 phase or M phase, 4',6-diamidino-2-phenylindole (DAPI) staining was employed, which is used to visualize the nuclei of cells. The nucleus of G_2 phase cells is singular and located at the joint between cell and bud, whereas M phase cells have two nuclei that are are distinctly separate while the cell and bud are still attached (34). The DAPI staining revealed that >90% of the large-budded *rad52* cells were in G_2 phase. The high levels of G_2 cells were found to be dependant on the presence of a functional DNA damage-response cell cycle checkpoint system, i.e., double mutants with both *RAD52* and known DNA damage checkpoint genes inactivated did not show the high G_2 cell phenotype. Additional microscopy work determined that *rad52* mutant cells grown to mid-log phase tend to be larger than WT cells, averaging about 1.5 μm larger in diameter. *rad52* cells were also shown to grow at a slower rate than WT cells. The growth rate experiments were carried out with both *MATa* and *MATα* cells and *rad52* cells were consistently found to have unusually long doubling times, primarily due to excessive amounts of time spent in G_2.

Goals of the current thesis project:

Initial work followed up on research conducted by Ms. Weis analyzing the high percentages of large-budded cells and slow rates of growth in *rad51* and *rad52* mutants compared with WT cells. It was determined that both *rad51* and *rad52* cells displayed a higher percentage of large-budded cells during mid-log phase and had longer doubling

times than WT cells. It is likely that inefficient repair of spontaneously occurring DSBs in *rad51* and *rad52* cells leads to a constitutively activated DNA damage checkpoint response which causes the cells to spend excessive time in G_2 phase.

The first steps of HR involve the resectioning of DSB ends to generate long ssDNA tails to which the filamentous Rpa complex can bind (Figure 2). This end processing is achieved by the actions of nucleases such as Mrx, Sae2, Exo1, the Sgs1-Dna2 complex, and possibly other proteins such as Top3 and Rim1. The possibility that these nucleases are required to generate ssDNA tails at spontanious DSBs that activate the checkpoint response in *rad52* cells was investigated. This was done by generating knockout mutants lacking one gene alone, or using double mutants. Example mutants included *exo1 rad52, sgs1 rad52, sae2 rad52,* and *srs2 rad52* cells. Their percentages of large-budded cells during mid-log phase growth were determined using phase contrast microscopy. The data indicated that deletion of *SAE2, SGS1,* or *EXO1* fail to reduce the elevated level of large-budded cells when combined with a *RAD52* knockout. Rmi1 and Top3 form a complex with Sgs1 thought to be involved with resection (32). However, *rmi1* and *top3 rad52* double knockout mutants also fail to reduce the elevated large-budded cell levels.

Previous work by Monica Weis established that the high level of large-budded cells in *rad52* mutant cultures was due to constituitive activation of the DNA damage checkpoint (44). This was done by knocking out *RAD52* in *mec3, dun1, ddc1, rad9, chk1, rad24,* and *rad17* mutants. During log phase growth *dun1 rad52* and *chk1 rad52* cultures contained a level of large-budded cells slightly above the WT average, and the others contained a level of large-budded cells consistant with the WT average. This was a strong

indication that the high levels of large-budded cells in log phase *rad52* cell cultures is due to constituitive activation of the DNA damage checkpoint.

A recent report indicated that Rad52 may play a role in the spindle assembly checkpoint (40). The possibility that defects in the spindle assembly checkpoint might be the cause of the high levels of large-budded cells was tested by creating *rad52 mad1* and *rad52 mad2* double mutants and growing them to mid-log phase, then examining their levels of large-budded cells. The double mutants had even higher levels of large-budded cells compared to *rad52* single mutants, suggesting that the cause of the large-budded cells was different in *rad52* vs *mad1/2* mutants.

Physical properties of *rad52* mutants such as light scattering effects, cell sedimentation rates, and electrical conductivity were also explored. Visible light spectroscopy was utilized to examine both the light scattering effects of *rad52* cells in comparision to WT cells, and also to examine the relative rates of sedimentation of the cells out of solution. It was determined that stationary phase WT and *rad52* cells sediment at similar rates, but mid-log phase *rad52* cells sediment out of solution significantly faster than WT cells. Both stationary and mid-log phase *rad52* cells displayed higher light scattering effects than WT cells, and each strain displayed higher light scattering effects during mid-log phase than they did during stationary phase. No significant difference was seen between the conductivity of solutions of WT cells vs *rad52* cells. These experiments were important because they demonstrated previously unreported phenotypes associated with DNA repair mutants, some or all of which may be common to all eukaryotic cells that are deficient in DSB repair.

ROS are known to be a source of damage to DNA (11). The role played by

oxidative chemicals in both spontaneous DNA damage and pausing in G_2 in *rad52* cells was analyzed by growth of the cells in media containing one or more well-studied antioxidants. Growth on YPDA plates containing N-acetylcysteine (NAC) followed by growth to mid-log phase in liquid YPDA containing the same concentration of NAC revealed no significant impact on G_2 phase arrest in either WT or *rad52* cells. The results suggest that oxidative damage to DNA leading to DSBs is not the major source of G_2 phase arrest in *rad52* cells.

II. MATERIALS AND METHODS

Equipment and Software

Horizon 11-14 gel rigs were purchased from LabRepCo (Horshan, PA). The Sorvall Lynx 6000 floor centrifuge, Savant DNA 120 SpeedVac Concentrator, replica-plating tool, and velvet squares were purchased from Thermo Fisher Scientific (Fair Lawn, NJ). The MXX-123 analytical balance was purchased from Denver Instruments (Bohemia, NY). All vortexes and incubators were purchased from VWR Scientific Products (Radnor, PA). The model 5424 centrifuge was purchased from Eppendorf (Hamburg, Germany). The RED imaging system was purchased from Alpha Innotech (San Jose, CA). The E19 Class shaker, Orbit Environ shaker, and Lab Rotator were purchased from Lab Line Instruments (Tripunithura, India). The orbital shaker and digital dry baths were purchased from BioExpress (Kaysville, UT). The model M837T phase contrast microscope was purchased from United Scope (Hopewell Junction, NY). The 2720 Thermal Cycler was purchased from Applied Biosystems (Foster City, CA). The T100 Thermal Cycler was purchased from Bio-Rad (Hercules, CA). The Vibracell CV18 was purchased from Sonics (Newton, CT). All graphs were made in Excel by Microsoft (Redmond, VA).

Reagents

Ethylenediaminetetraacetic acid (EDTA) and sodium hydroxide (NaOH) were purchased from EMD Chemicals, Inc. (Darmstadt, Germany). Dimethyl sulfoxide (DMSO) and lithium acetate (LiAc) were purchased from Alfa Aesar (Heysham, Lancashire). Sodium dodecyl sulfate (SDS) was purchased from J.T. Baker (Center Valley, PA). Anhydrous sodium acetate and glacial acetic acid were purchased from

Mallinckrodt-Baker, Inc. (Paris, KY). Sonicated salmon sperm carrier DNA was purchased from Agilent Technologies (Santa Clara, CA). Ethidium bromide (EtBr) was purchased from IBI Scientific (Peosta, IA). Sodium chloride, sodium citrate dihydrate, Tris-HCl, and Phusion DNA polymerase were purchased from ThermoFisher Scientific (Fair Lawn, NJ). Ammonium sulfate and isopropanol were purchased from VWR International (West Chester, PA). Boric acid, maleic acid, and polyethylene glycol (PEG 4000) were purchased from Sigma-Aldrich Chemical Co. (St. Louis, MO). Agarose LE was purchased from Gold Biotechnology (St. Louis, MO). TAE (50X) buffer was purchased from Omega (Cowpens, SC). Ethanol was acquired from Texas State University (San Marcos, TX). RNase A was purchased from Sigma-Aldrich Chemical Co. (St. Louis, MO). Restriction enzymes NotI-HF and ApaI, dNTPs, $MgCl_2$, Phusion HF, 5x Phusion buffer, 6X loading dye, and 2 log DNA ladder were purchased from New England Biolabs (Beverly, MA). Integrated DNA Technologies (IDT) (Coralville, IO) or ThermoFisher Scientific-Life Technologies Corporation (Grand Island, NY) synthesized all primers. All amino acids, and ampicillin (Amp) were purchased from Sigma-Aldrich Chemical Co. (St. Louis, MO). D-(+)-glucose, soy peptone, and yeast nitrogen base were purchased from Amresco (Solon, OH). Bacto yeast extract was purchased from Becton, Dickinson, and Company (Sparks, MD). Molecular biology grade agar was purchased from Teknova (Hollister, CA). QIAprep Spin Miniprep Kits were purchased from Qiagen (Hilden, Germany). Phosphate Buffered Saline 10X liquid concentrate was purchased from OmniPur (Gibbstown, NJ).

Yeast strain backgrounds used for this project were BY4741 and BY4742 (45). Plasmid pΔ52L was used to perform deletion-disruption of the *RAD52* gene. The plasmid

was cut with NotI-HF and ApaI restriction enzyme before being used to transform yeast cells. All yeast strains employed or created for this project are listed in Table 1. All DNA oligonucleotides used in the study are listed in Table 2.

Table 1. *S. cerevisiae* strains used

Strain Number	Strain description	Source
BY4741	*MATa ura3Δ0 leu2Δ0 met15Δ0 his3Δ1*	(45)
BY4742	*MATα ura3Δ0 leu2Δ0 lys2Δ0 his3Δ1*	(45)
YLKL689	BY4742, *rad52Δ::LEU2*	Lab strain
YLKL782	BY4742, *rad52Δ::URA3 sae2Δ::HygB^r*	Lab strain
YLKL1616	BY4742 *mad1Δ::G418^r* library strain, but *rad52Δ::LEU2*	Lab strain
YLKL1617	BY4742 *mad2Δ::G418^r* library strain, but *rad52Δ::LEU2*	Lab strain
YLKL1620	BY4742, *rad52Δ:LEU2 DDC2-GFP::HIS3*	This work
YLKL1621	BY4742, *rad52Δ:LEU2 RFA1-GFP::HIS3*	This work
YLKL1630	BY4742 *sae2Δ::G418^r* library strain, but *rad52Δ::G418^r*	This work
YLKL1631	BY4742 *exo1Δ::G418^r* library strain, but *rad52Δ::G418^r*	This work
YLKL1632	BY4742 *sgs1Δ::G418^r* library strain, but *rad52Δ::G418^r*	This work
YLKL1649	BY4741 exo1*Δ::G418^r* library strain, but *rad52Δ::G418^r*	This work
YLKL1650	BY4741, sgs*1Δ::G418^r* library strain, but *rad52Δ::G418^r*	This work
YLKL1651	BY4742 *rmi1Δ::G418^r* library strain, but *rad52Δ::G418^r*	This work
YLKL1652	BY4742 *top3Δ::G418^r* library strain, but *rad52Δ::G418^r*	This work
YLKL1659	BY4742, *sgs1Δ::G418^r*	This work
YLKL1660	BY4742, *exo1Δ::G418^r*	This work
YLKL1665	BY4742 *sgs1Δ::G418^r* isolate 1, but *rad52Δ::LEU2*	This work

Table 1 (cont.)

Strain Number	Strain description	Source
YLKL1666	BY4742 *sgs1Δ::G418*^{r} isolate 7, but *rad52Δ::LEU2*	This work
YLKL1667	BY4742 *exo1Δ::G418*^{r} isolate 1, but *rad52Δ::LEU2*	This work
YLKL1668	BY4742 *exo1Δ::G418*^{r} isolate 8, but *rad52Δ::LEU2*	This work

Table 2. Polymerase chain reaction (PCR) primer sequences

Primer Name	Primer Sequence
tRad52E	GTC AGC GTC AGT GAC ATG ATG TTG TAG GTT GTA
Leu2A	TCC AGC GCC TCA TCT GGA AGT GGG ACA C
5-SgsC	GAA GAG AAG CTT CTC TCC ACA TGT CCT TTA TAT
3-SgsD	GAA TTT AAT ATG TAC ATG CCC TTC TGT AGA AGA
5-Sgs	CGA GCC TGA TCT AAA AGC TGA TAT ACG GAT CA
3-Sgs	GAA GTT GAT AAC TGA GCA ATG TGC ACA CCA CA
G418b	CAT GTT TCA GAA ACA ACT CTG GCG CAT CG
5-ExoC	CTG AGG TTG ACT ACT ACG AGC TAT ACG AAT ATC
3-ExoD	GGC AAA CAT ACT TGT GGC TTA ATT TGA CAC ATC
5'exo1	CCG AGA AGG AGA AGT ATT ACG TCC
3'exo1	CGT ACC CTG TCC TAC TTT ACT GG

Media and Solutions for Cell Cultures

YPDA solid media was made according to the procedures set out by Sherman, (yeast extract, soy peptone, glucose, agar, adenine, and dH_2O) with the exception of using soy peptone rather than bacto-peptone, and 0.001% adenine instead of 0.003% (46). YPDA liquid broth was made in the same way, except for the absence of the 2% agar. Selective YPDA plates were made as above but with the addition of 250 μg/mL G418 or 300 μg/mL Hygromycin B (HygB). Selective synthetic media contained 0.17% yeast nitrogen base without ammonium sulfate or any amino acids, 2% glucose, 2% agar, 0.5% ammonium sulfate, as well as all essential amino acids required for strain selection.

Agarose Gel Electrophoresis

Horizon 11-14 gel rigs containing 1X TAE (40 mM Tris, 20 mM acetic acid, 1 mM EDTA) buffer were used to run 0.6-0.9% agarose gels anywhere between 60V and 130V. Gels were stained after running in 0.5 μg/mL ethidium bromide (EtBr) and then visualized on an Alpha Innotech Red Imaging System.

Chromosomal DNA Minipreps

All yeast chromosomal DNA minipreps were done according to the protocol developed by Lee *et al.* (47). YPDA cultures containing 4 mL were grown overnight while being shaken at 30°C. Aproximately 1.5 mL of each culture was added to a microfuge tube and it was centrifuged at 10,000 x *g* for 10 s. Then the supernatant was discarded. To the same tube approximately 1.5 mL of additional overnight culture was added and the tube was spun and the supernatant discarded as before. Next, 300 μL SET* (6% SDS, 10 mM EDTA, plus 30 mM Tris [pH 8.0]) was used to resuspend the cell

pellet before a 15 min incubation at 65°C or 5 min incubation at 75°C, either one followed by a 5 min incubation in wet ice. After that, 150 μL of cold 3 M potassium acetate (KOAc) was added and the tubes were hand-shaken for ~10 s, then centrifuged at 21,000 x *g* for 10 min. The supernatant was then transferred to a new microfuge tube and 500 μL of isopropanol was added. The tube was shaken by hand vigorously then centrifuged at 21,000 x *g* for 1 or 2 min and the supernatant was removed. The DNA-containing pellet was washed with 200-500 μL of cold 70% ethanol (EtOH) for 1 min and then dried in a speedvac for 10 min. The dried pellet was suspended in 45-50 μL TE plus 1 μL of 2 mg/mL RNase A. Each tube was then incubated at 37°C for 10 min then at 4°C for at least 10 min to allow the chromosomal DNA to dissolve. Following this step, additional cleanup was sometimes performed, in which case tubes were spun at 21,000 x *g* for 2 min and the supernatant was transferred to a new tube.

Inactivation of genes in *S. cerevisiae* cells

DNA fragments transformed into cells were either inserted as PCR products or as fragments derived from restriction enzyme digestion of a plasmid. In each case the gene used for insertion was flanked at the 5' and 3' ends by several hundred bp of sequence with homology to a gene on a yeast chromosome. Transformations were carried out according to the Lewis lab protocol (48). A 1.5 mL aliquot of an overnight cell culture grown in 3-5 mL YPDA broth was transferred to a microcentrifuge tube and centrifuged at 2500 or 3000 x *g* for 15 s. Pellets were resuspended in 500 μL 0.1 M DTT and heated at 42°C for 20 min. The spin was repeated for 10 s and the supernatant discarded. To the pellet, 5 μL of 10 μg/mL sonicated salmon sperm DNA as well as 1-10 μL of transformation DNA was added. After vortexing, 500 μL of a mixture containing

polyethyline glycol (PEG), lithium acetate (LiAc), Tris and EDTA, along with 56 μL of dimethyl sulfoxide (DMSO) were used to resuspend the pellet. Tubes were incubated at 30°C for 15 min and then 42°C for 15 min. Afterwards, tubes were centrifuged at 2,500 x *g* for 15 s, the supernatant was removed, cells were resuspended in 1 mL YPDA broth and shaken at 30°C for ~1 h.

If cells were being transformed with a gene encoding resistance to G418, cells were centrifuged at 2,500 x *g* for 15 s then resuspended in 300 μL YPDA broth. A total of 150 μL was spread onto two different YPDA plates to make a lawn then grown for 1-2 days at 30°C or 3-4 days at room temperature. Afterwards, the lawn plates were replica plated to selective plates and colonies allowed to form over the next 2-3 days at 30˚C.

If the cells were not being transformed with G418 resistance genes, then pellets were resuspended in 200 μL dH_2O instead of 300 μL YPDA broth. After that, 10 μL of the cell solution plus 50-100 μL dH_2O was spotted and spread onto one selective plate, and 100 μL of the cell solution was spotted and spread onto another selective plate.

PEG/LiAC/Tris/EDTA solution was made using the following recipe for 1 mL of solution: 800 μL 50% PEG 4000 + 100 μL 1 M LiAc + 20 μL 50 mM EDTA + 10 μL 1 M Tris (pH 7.5) + 70 uL dH_2O.

Replica Plating and Streaking to Isolate Transformed Colonies

Replica plating was carried out when lawns were grown after transformation. A square piece of velvet cloth was secured to a replica plating tool and the lawn was firmly pressed against the velvet. A spacer plate was then pressed against the velvet square. A selective plate was then pressed against the same velvet square. After this, the velvet

square was replaced with a clean one and the process repeated with the next lawn and two new plates. The spacer and selective plates were then grown at 30˚C for 2-3 days or at room temperature for 4-5 days. Single colonies were numbered and streaked to new selective plates to purify them away from unstransformed cells on the original plates. The cells were then grown at 30˚C for 2-3 days or at room temperature for 4-5 days. At least two isolates which exhibited normal growth were then analyzed by PCR to confirm proper insertion of the selectible marker into the target gene.

Cell Cycle Phase Analysis and Multibudded Cell Counting by Phase Contrast Microscopy

A small amount of cells was transferred via toothpick to a microfuge tube containing 300 μL YPDA broth, then vortexed and a 1:40 dilution made by aliquoting from this microfuge tube into one containing 1 mL dH_2O. The 1:40 dilution was vortexed then sonicated for 15 s at 24% power to reduce cell clumping. Approximately 14 μL of the 1:40 dilution was loaded onto a hemocytometer and 3 squares were counted diagonally across the 25-square grid at the center. The volume of cells in mL needed to make a 1 mL YPDA cell culture with a titer of $3x10^6$ cells per mL was calculated with this equation:

$$\frac{3x10^6}{\text{mean \# cells per square} * 25 \text{ squares} * 10{,}000 * 40/1 \text{ dilution factor}} = \text{cell volume}$$

The 300 μL YPDA tube was vortexed and the calculated volume was aliquoted into four different 2 mL microfuge tubes containing 1 mL YPDA broth. All tubes were shaken for 6 h ± 15 min at 30°C. Tubes were then vortexed and sonicated as above. Aliquots of each cell solution were added to hemocytometers and a total of 100 cells

were counted in the long rows on the ends of the hemocytometers. The number of unbudded, small-budded, and large-budded cells were tracked during the count to generate percentages. Final percentages were the mean of the four cultures of each strain. If the number of multibudded cells was analyzed, then 300 WT and 500 *rad52* cells were counted and the number of multibudded cells, and number of additional buds, were noted. If cells were too concentrated for swift and accurate counting, or counting was expected to take more than a few minutes, $1/4^{th}$ or $1/5^{th}$ dilutions into 1 mL dH_2O were proposed and then vortexed and sonicated before loading onto the hemocytometer as above.

Doubling Time Determination

Cell cultures at a concentration of $3x10^6$ cells/mL were started as per cell cycle phase analysis above. Cell titer was analyzed every hour starting at the three hour mark and going to at least the seven hour mark. For the hour five timepoint, the third timepoint analyzed, a 60 µL aliquot of cells was added to 240 µL dH_2O to make a 1:5 dilution. This dilution was vortexed, sonicated, and the titer determined. For timepoints at six and seven hours, the dilution was changed to 1:10 in a total volume of 300 µL. For the eight hour timepoint, a 1:20 dilution was made in a final volume of 600 µL. Each time cells were only removed from the shaker long enough to take aliquots or load hemocytometers. The means of four cultures of each strain were used to generate plots of cell titer vs time. Best fit trendlines were used to calculate doubling times.

Cell Size Determination

A small amount of WT or *rad52* cells were transferred to a microcentrifuge tube using a toothpick, suspended in dH_2O, and loaded on a hemocytometer and viewed with a

phase contrast microscope. For the WT, 15 unbudded and 15 budded cells were counted. The same was done for the *rad52* mutant. The maximum length of the cell was counted using tick marks in the ScopeImage DynamicPro version 1.0 software. These measurements were converted to μm with a conversion factor of 1.7. Their means and standard deviations were calculated using Microsoft Excel. Their distributions were calculated using the Excel formula and the μm data:

=NORM.DIST(cell size, mean size, standard deviation, FALSE)

The data for log phase cell sizes was collected as detailed by Monica Weis (44).

PCR Analysis of Purified Chromosomal DNA

PCR reactions were typically run using a mixture as follows:

- 23 μL dH_2O
- 5 μL Primer 1
- 5 μL Primer 2
- 4 μL 2.5 mM dNTPs
- 9-10 μL 5x Phusion buffer
- 0.7-1.0 μL Phusion polymerase
- 2 μL chromosomal DNA

PCR reactions were run using instrument settings as follows:

- 94°C 2 min
- 94°C 2 min
- 48-55°C 2 min
- 72°C 1-2 min

(34 cycles)

- 72°C 7 min
- 4°C ∞

Results of PCR reactions were examined by running 2-5 μL of the product on 0.6-0.9% agarose gels. PCR was used both to isolate DNA to carry out a transformation and to determine the success of a transformation. The successful creation of a *rad52Δ::LEU2* mutant was confirmed using the tRAD52E and Leu2A primers. *exo1Δ::G418*^{r} mutants

were confirmed using 5-ExoC and G418b primers. Similarly, *sgs1Δ::G418*^{r} mutants were confirmed using 5-sgsC and G418b primers. Producing a selectable marker gene-containing fragment to use for transformation used primers containing sequences of homology to the gene to be knocked out. Of the multiple primers used for amplification of an *exo1Δ::G418*^{r} chromosomal DNA fragment, 5-ExoC and 3-ExoD were found to work the best. Likewise, 5-SgsC and 3-SgsD performed best for amplification of sequences from *sgs1Δ::G418*^{r}. In each case, 5 corresponds to the upstream primer and 3 to the downstream primer.

Alternative PCR with Yeast Cells from Overnights or Colonies

An alternative method of obtaining chromosomal DNA for PCR was also used. The Kristjuhan *et al.* protocol was used with modifications (49). For an overnight culture, 100 µL of YPDA liquid cell cultures with an OD_{600} of 0.9-2.2 was used. These cells were spun down and resuspended in 400 µL 200 uM LiAc/1% SDS solution. Cells were resuspended at the end of the procedure in 45-50 µL TE. When taking cells directly from a plate, small numbers of cells were taken from streaks using toothpicks rather than picking from isolated colonies. The 70% EtOH wash step was carried out with cold ethanol which was allowed to remain in the microfuge tubes for 1 min before being removed. After this step, the tubes were placed upside down, with the lids open, on layered Kimwipes and allowed to air dry for at least twenty minutes.

Preparation of FACS Samples

S. cerevisiae cells were grown in 1 mL YPDA liquid culture for 6 h. Cells were then collected at a titer of $1x10^7$ cells/mL and spun down at 3000 x *g* for 15 s. The pellet

was resuspended in 300 µL H_2O by vortexing. Afterwards 700 µL EtOH was added, the solution was vortexed again, then kept at 4°C overnight. Cells were again spun down at 3000 x *g* for 15 s, the supernatant was discarded, the tubes quick spun, the residual supernatant discarded, and the pellet resuspended in 100 µL 50 mM sodium citrate, pH 7.0. Next, 10 µL of 10 mg/mL RNaseA was added and the solution was vortexed and incubated at 50°C for 2 h. Afterwards, 5 µL of 20 mg/mL Protease K was added and the tubes were incubated at 50°C for 1 h. Cells were spun down and resuspended in 500 µL 1x phosphate-buffered-saline (PBS). Next 8 µL of 1 mg/mL potassium iodide was added to the tube. The tubes were then vortexed, covered with foil and/or kept in a drawer to block light, then kept at room temperature for 25 minutes or 4°C for up to overnight. Tubes were then sent via FedEx to the University of Texas Health Science Center San Antonio Flow Cytometry Core Facility for analysis on the BD Calibur flow cytometry instrument. This project was supported by the Flow Cytometry Facility at UTHealth San Antonio with funding from University and the NIH (NCI P30 CA054174).

III. RESULTS AND DISCUSSION

Recent work in this lab by Monica Weis demonstrated that DSB repair-deficient *rad52* mutants have several unusual properties (44). They are larger than normal cells, on average, and they contain a higher percentage of large-budded G_2 phase cells when grown in liquid cell culture. The high level of G_2 cells was restored to normal when genes required for activation of DNA damage-induced cell cycle checkpoints were also inactivated. This result suggested that *rad52* cells have constitutively activated DNA damage checkpoint responses, likely due to the presence of unrepaired spontaneously occurring double-strand breaks in the DNA of the mutant cells. Other homologous recombination-deficient mutants such as *rad51*, *rad54*, *rad55*, *rad57*, and *rad59* strains also exhibited high levels of G_2 cells in liquid culture, suggest that they also have frequently activated DNA damage checkpoints.

By analyzing log phase WT and *rad52* cultures with phase contrast microscopy as well as DAPI staining and fluorescence microscopy the percentage of cells in each of the four phases of the cell cycle at any time during their growth can be determined. The average time it takes for a WT or *rad52* cell to pass through all four phases can be found experimentally by plotting cell titer vs time. The equation of the generated line can then be used to calculate how long it took a cell culture's concentration to double. The percentage of cells in each step of the cycle and the time it takes an average cell to double can then be used to calculate how long an average cell spends in G_1, S, G_2, and M phase.

As shown in Figure 6a, Monica Weis was able to calculate the number of minutes WT and *rad52* cells spend in G_1, S, and G_2+M combined. The times spent in G_1 and S were similar, but the times spent in G_2+M were very different. As part of the

current project, I used her DAPI stain data to distinguish time in G_2 from time in M phase. As shown in Figure 6b, times spent in M were also similar in WT and *rad52* cells, but times spent in G_2 were dramatically different. WT cells spent 17.7 min in G_2 while *rad52* cells spent 59.9 min. Thus, *rad52* mutants spend 3.4 times longer in G_2 phase.

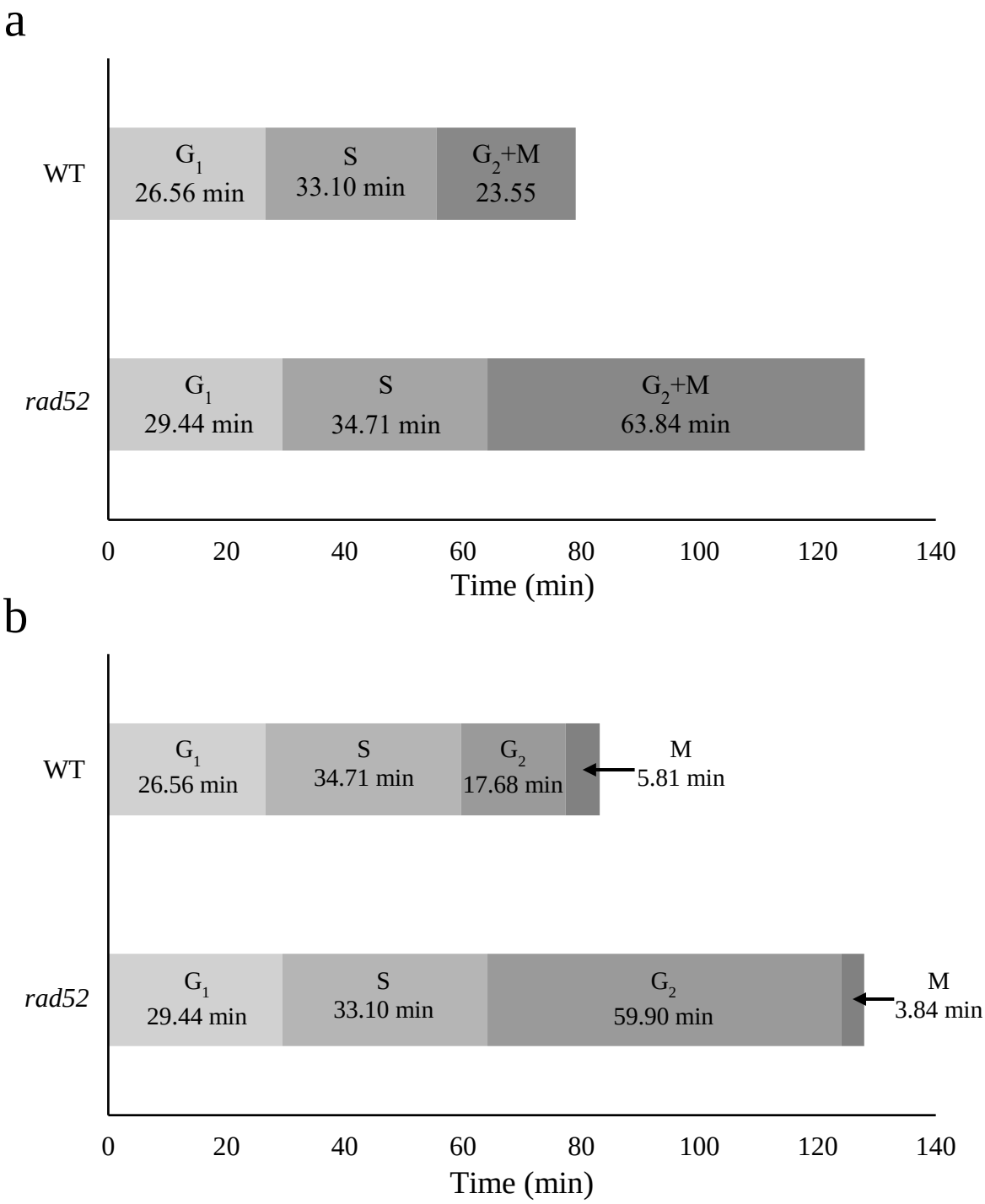

Figure 6. Time spent by WT and *rad52* cells in each cell cycle phase. a) Times in the phases determined with data gathered from phase contrast microscopy and doubling time experiments. b) G_2+M data was split into G_2 and M thanks to DAPI determination of percentage of cells in G_2 and percentage of cells in M phases.

Monica Weis carried out doubling time experiments on HR-deficient *rad52* mutants and compared their rates of growth with WT cells and found that *rad52* cells took 1.5 times longer to complete a cell cycle. However, she could not get unambiguous data for *rad51* mutants, which are also strongly deficient in HR. Part of the initial work on my project was to follow up on her research. This was done by re-examining growth rates in WT, *rad51*, and *rad52* cells. Cells were inoculated into 1 mL YPDA broth cultures at starting titers of $3x10^6$ cells/ml at 30°C while shaking. Every hour, starting at the third hour, cell titers were determined by counting cells on a hemocytometer. Cell titer versus time plots in Excel were used to calculate the time required for the concentration of cells in each strain to double in number (Figure 7a). Both *rad51* and *rad52* strains had slower doubling times than WT cells. Out of both mutant strains, *rad52* cells had the slowest doubling time at 104 minutes, versus 82 minutes for *rad51* cells and 73 minutes for WT cells (Figure 7b).

a

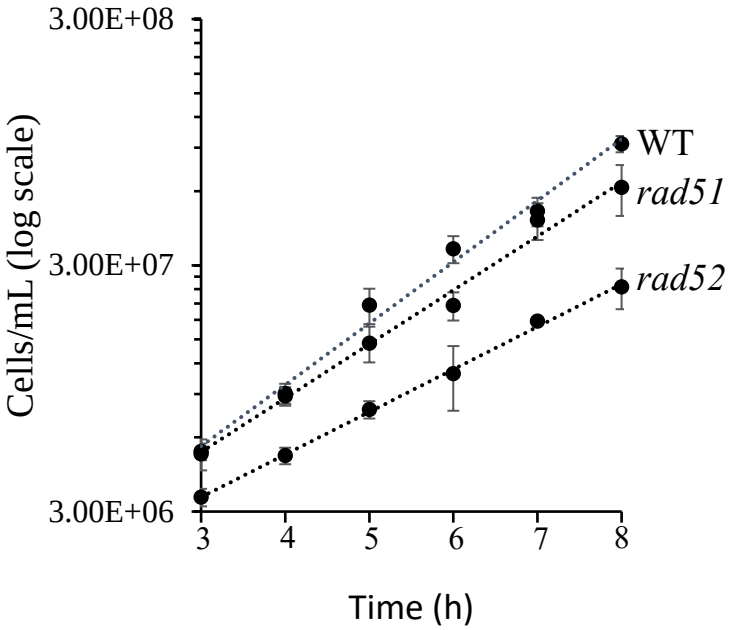

b

Strain	Doubling Time (min)
WT	72.6
rad51	82.2
rad52	104.4

Figure 7. Doubling times of WT, *rad51*, and *rad52* cells. a) A graph of average cell titer versus time. b) *rad51* cells' doubling time was 13.2% greater than that of WT cells. *rad52* cells doubling time was 43.8% greater than in WT cells.

Many *rad52* mutant cells appear larger than WT cells when viewed using phase contrast microscopy. Examples of WT and *rad52* cells that I analyzed at 400x magnification are shown in Figure 8a and 8b. To further explicate the work Monica Weis did with *rad51* mutants, I determined the percentages of large-budded cells for mid-log phase WT, *rad51*, and *rad52* cell cultures. Approximately 28% of WT cells were large-budded (G_2/M) after six hours of shaking in YPDA broth (Figure 8c). By contrast, *rad51* and *rad52* mutant cultures had 44% and 49% large-budded cells, respectively. *rad52* trended higher than *rad51*, but their difference was not statistically significant

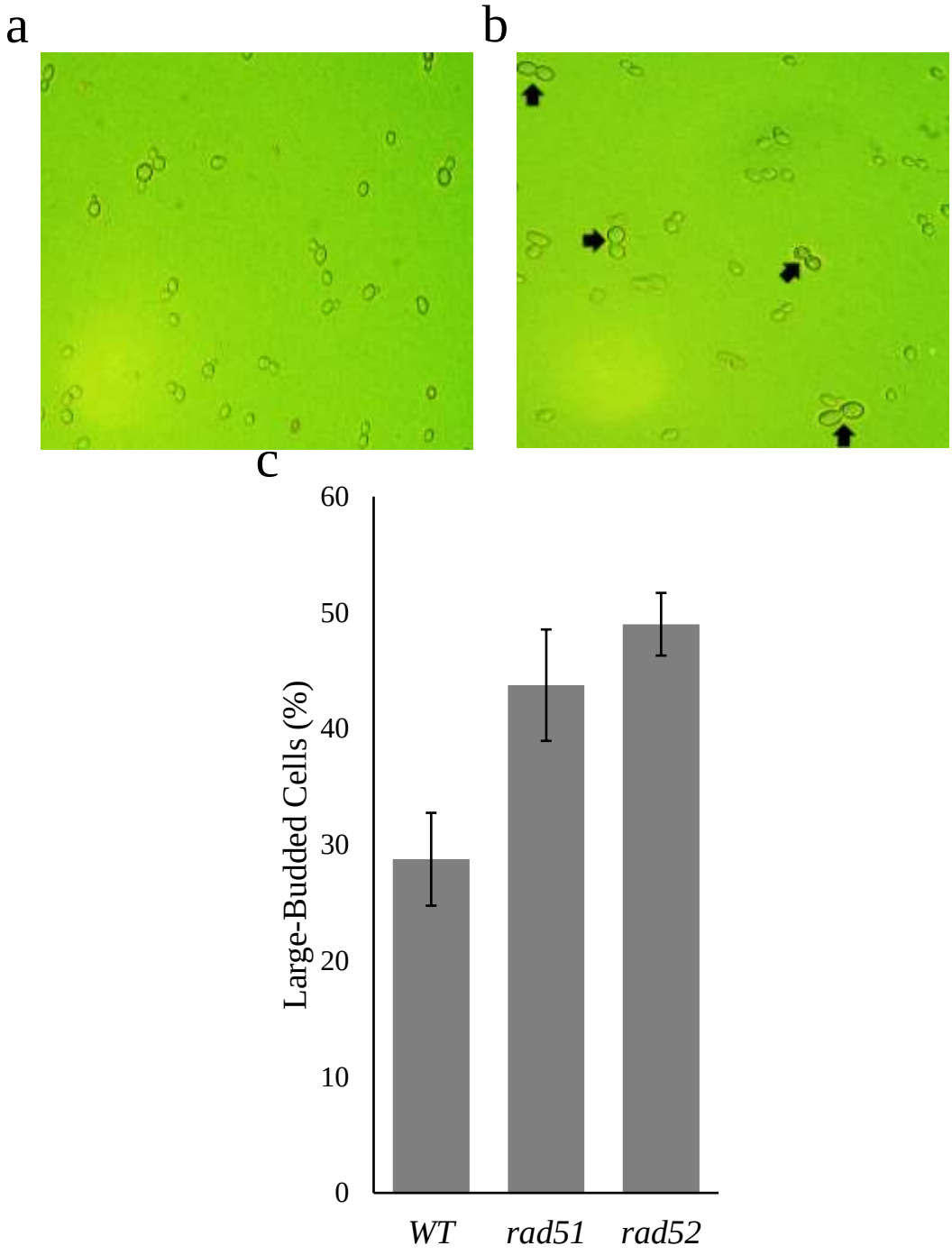

Figure 8. Differences in large-budded cell appearance and number during log phase growth. a) WT cells during mid-log phase growth at 400x magnification on a phase contrast microscope. b) *rad52* cells during mid-log phase growth at 400x magnification on a phase contrast microscope. Note both the larger size of some *rad52* cells as well as the increased percentage of large-budded cells. c) Percentage of large-budded G_2/M cells in WT and mutant populations. *rad51* and *rad52* are HR deficient and display a higher percentage of G_2/M cells. Average of four replicates are shown. Error bars indicate standard deviations.

Former graduate student Monica Weis quantified cell sizes in mid-log phase WT and *rad52* cells. Her work was followed-up in this project with data collected from stationary phase WT and *rad52* cells. Log phase cultures have approximately equal numbers of G_1, S, and G_2/M cells. By contrast, stationary phase cultures typically contain $\geq$ 90% unbudded G_1 phase cells. As both stationary and log phase cells are frequently utilized in this field, we deemed it important to collect data on both these phases. The maximum diameters of cells were analyzed at 400x magnification by phase contrast microscopy with a length scale overlaid over each field of cells. Because unbudded G_1 phase yeast cells are smaller than budded S and G_2/M cells, the sizes of unbudded and budded cells were measured separately.

When the unbudded cells were examined during stationary and mid-log phase, similar trends were seen. Among stationary phase cells, unbudded *rad52* cells were larger than unbudded WT cells (6.8 vs 5.8 μm) and budded *rad52* cells were larger than budded WT cells (7.1 vs 6.1 μm) (Table 3). These results are similar to those of log phase cells observed by Monica Weis. She determined that, among log phase cells, unbudded *rad52* cells were larger than unbudded WT cells (6.7 vs 5.3 μm) and budded *rad52* cells were larger than budded WT cells (8.3 vs 6.8 μm) (Table 3).

Table 3. Maximum cell diameter means and ranges

Strain and Growth Phase	Unbudded Mean Size (μm)	Unbudded Size range (μm)	Budded Mean Size (μm)	Budded Size range (μm)
WT Stationary	5.8	5.1-6.8	6.1	3.4-7.7
WT Log	5.3	4.3-7.2	6.8	4.8-9.6
rad52 Stationary	6.8	5.4-7.7	7.1	5.1-9.4
rad52 Log	6.7	4.8-9.6	8.3	6.0-12.3

The distributions of cell sizes were also analyzed. Although the average size of unbudded *rad52* cells was larger than that of WT cells, many of the *rad52* cells fell within the same size range as WT cells (Figure 9a and 9b). This was also true for budded *rad52* cells (Figure 10a and 10b). The range of sizes of log phase *rad52* cells was large (4.8 to 9.6 μm for unbudded cells and 6.0 to 12.3 μm for budded cells). This large range is evident in Figures 9b and 10b, where it is seen that the range of sizes for *rad52* cells is much larger than that of WT cells.

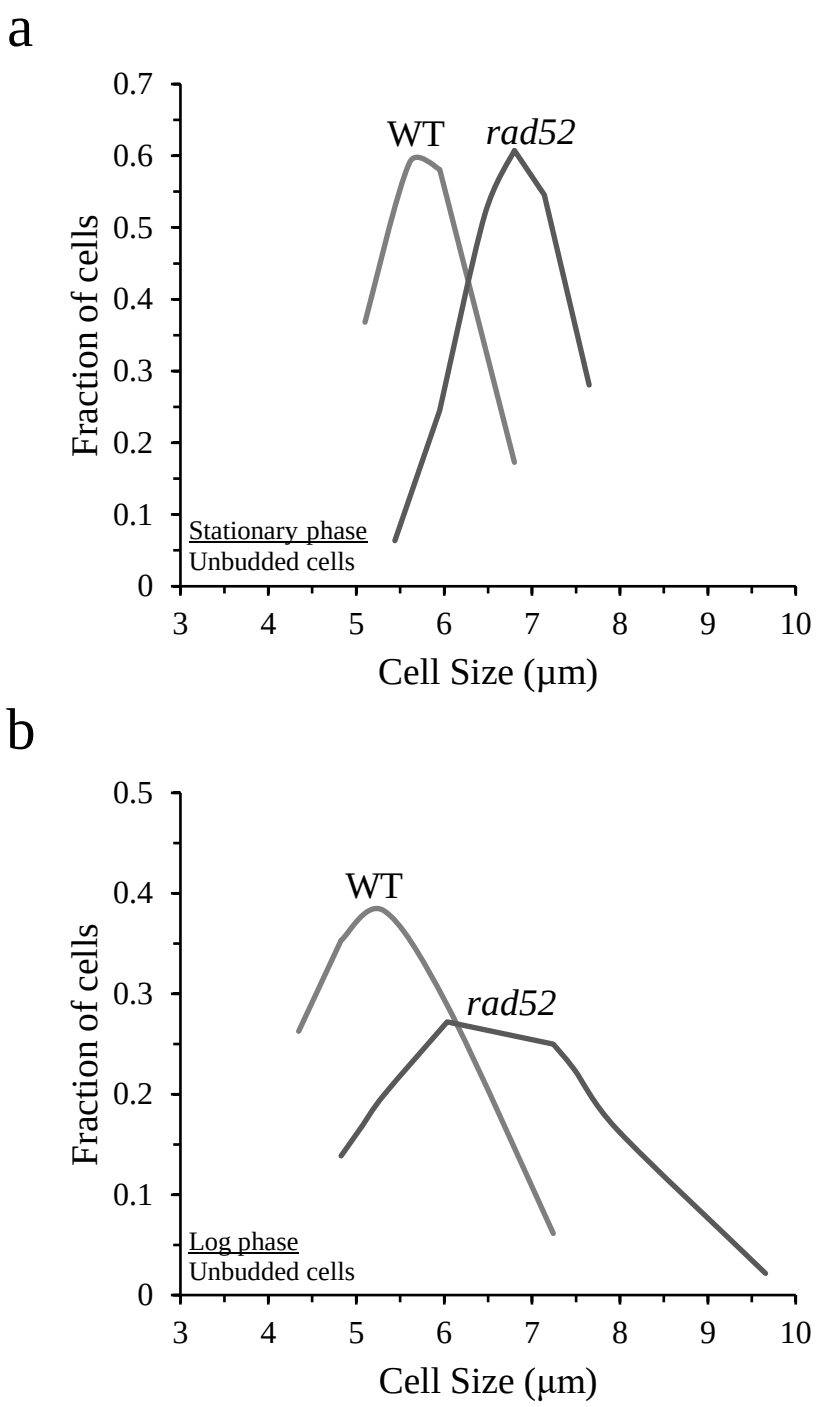

Figure 9. Cell diameter distributions for stationary and mid-log phase unbudded WT and *rad52* cells. a) During stationary phase *rad52* cells have larger average diameters than WT cells. b) Monica Weis determined that during mid-log phase unbudded *rad52* cells were larger than WT cells and possessed a wider distribution of sizes.

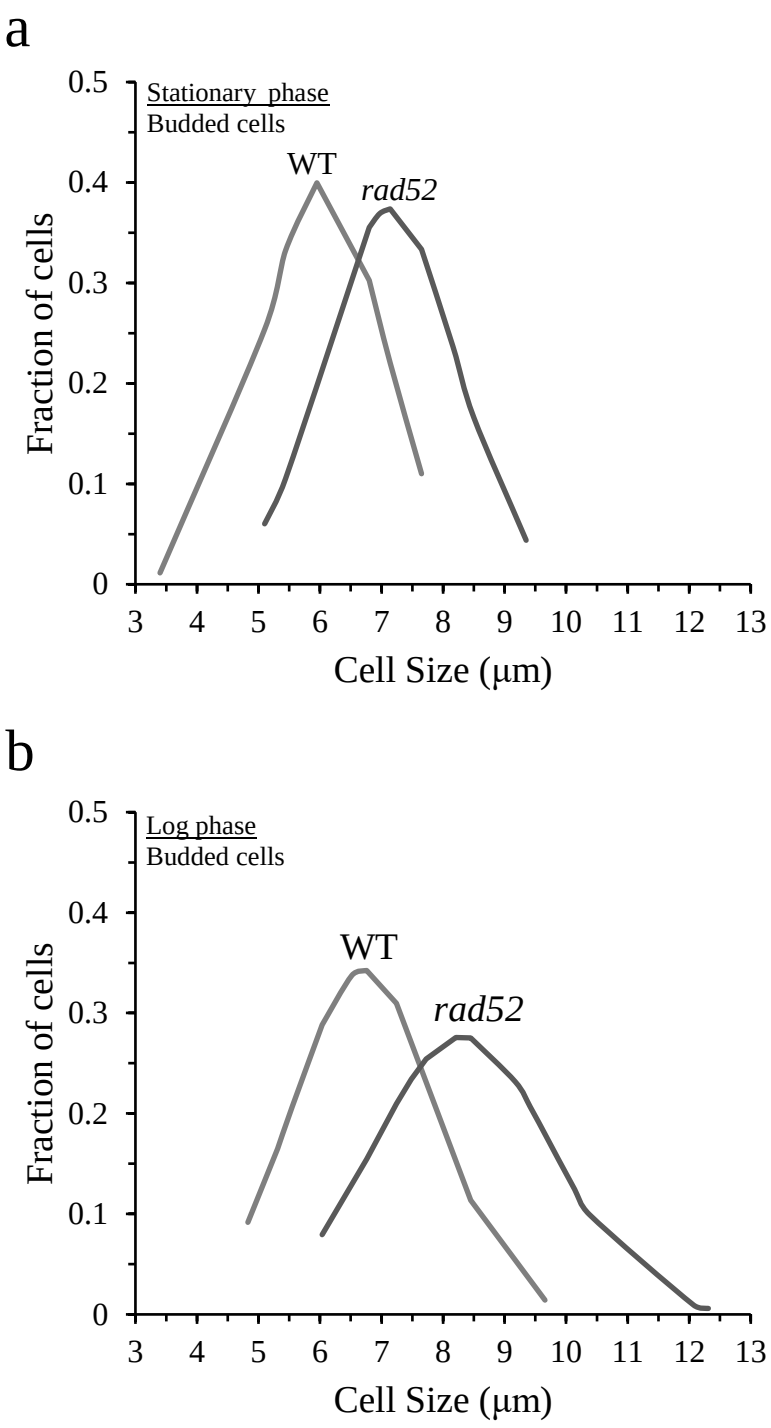

Figure 10. Cell diameter distributions for stationary and mid-log phase budded WT and *rad52* cells. a) During stationary phase *rad52* cells have larger diameters than WT cells. b) Monica Weis determined that during log phase unbudded *rad52* cells were larger than WT cells and demonstrated a wider distribution of sizes.

As a budding yeast, each *S. cerevisiae* cell typically produces a single bud at a time while reproducing. Occasionally cells with more than one bud will be seen, which is an aberration indicating that the timing and coordination of cell cycle events has become altered. These cells are termed multibudded cells and can exist with one or more buds present, either all originating from a central cell or with one or more buds coming off another bud (Figure 11a and 11b). WT and *rad52* cultures of both mating types, *MATa* and *MATα*, were examined for multibudded cells. *MATa rad52* cultures had 3 times as many multibudded cells as *MATa* WT cells (Figure 11c). Among *MATα* cells, *rad52* mutants exhibited twice as many multibudded cells as WT cells. For each analysis, four replicates 300 WT cells and 500 *rad52* cells were counted. The results indicated a trend of *rad52* mutants possessing a higher percentage of multibudded cells, possibly due to the higher level of cells undergoing a DNA damage-induced stress response.

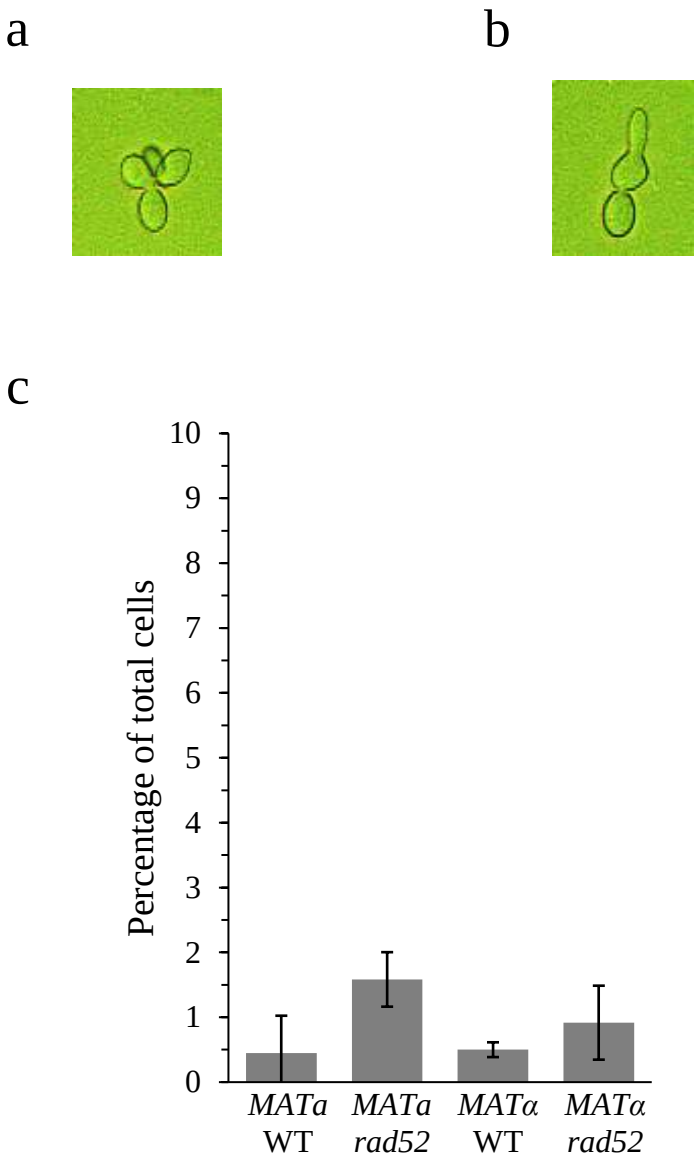

Figure 11. Multibudded cells in mid-log phase cultures. a) Example of a clustered multibudded cell. b) Example of an extended multibudded cell. c) Percentages of multibudded cells during mid-log phase growth. A total of 500 WT cells were counted for each mating type, and the results of four counts of each were averaged. A total of 300 *rad52* cells were counted for each mating type, and the results of four counts of each were averaged. Error bars represent standard deviations.

Fluorescence-activated cell sorting (FACS) is a method of automatically sorting or counting cells one at a time based on their fluorescent intensity (50). When chromosomal DNA is stained with a fluorophore, FACS can be used to determine the relative numbers of cells that have haploid (1n) DNA content versus diploid (2n) DNA content. This corresponds to the number of cells that are in G_1 phase versus G_2/M. Due to the propensity of *rad52* cells to pause during G_2, mid-log phase WT and *rad52* cells were examined using FACS. WT *MATα* cells showed approximately equal amounts of cells with G_1 and G_2/M DNA content (Figure 12a). By contrast, *MATα rad52* cells exhibited much greater numbers of cells with G_2/M DNA content (note the tall second peak in Figure 12b). Similar results were seen in *MATa* WT and *rad52* cells (Figure 12c and 12d). The *rad52* strains of both mating types were seen to have a higher number of cells in the second peak, which is consistent with the higher percentage of large-budded cells seen using phase contrast microscopy.

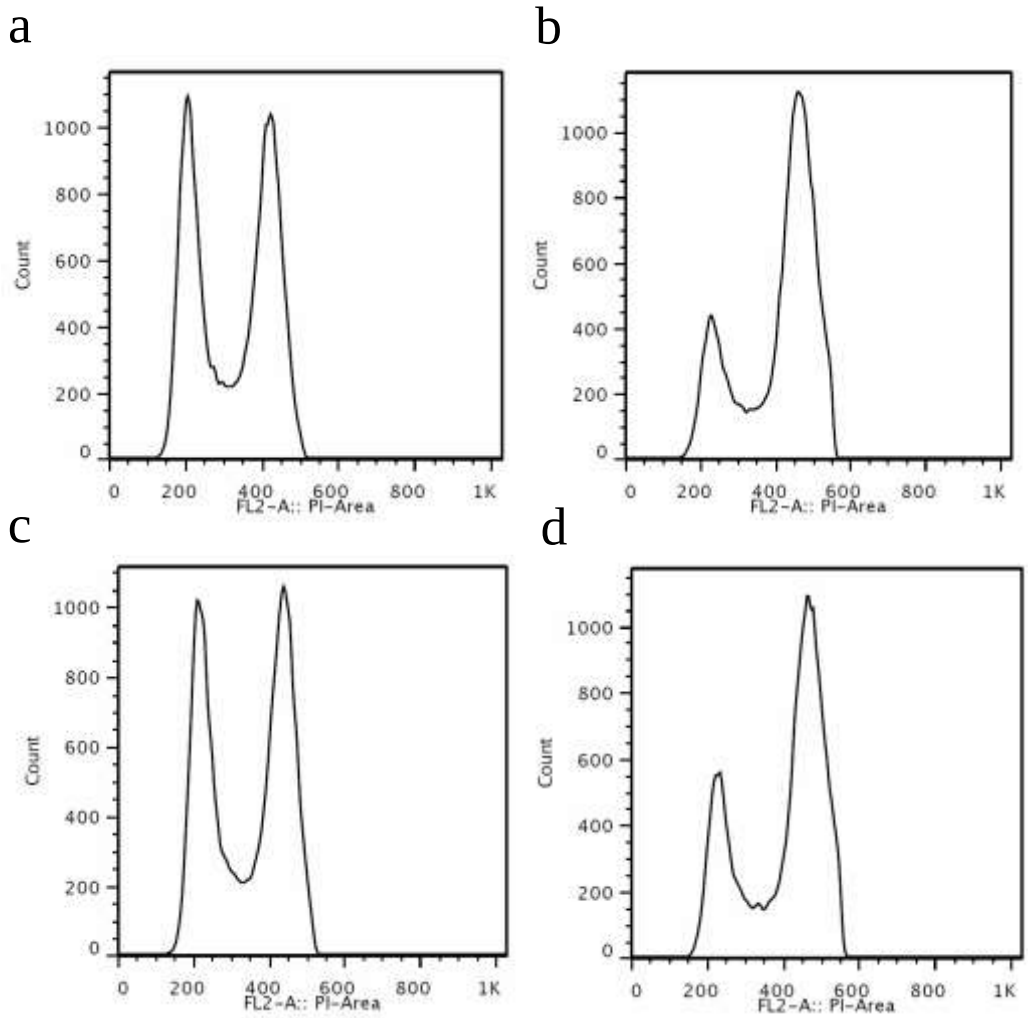

Figure 12. FACS histograms revealed relative amounts of DNA inside cells. The first peak in all four graphs represents the relative number of cells with G_1 phase DNA content. The second peak represents the fraction of cells with G_2/M phase DNA content. a) *MATα* WT. b) *MATα rad52*. c) *MATa* WT. d) *MATa rad52*.

Spectrophotometry is a common biochemical technique. It can be used to measure either the amount of light absorbed or scattered at a certain wavelength in aqueous solutions. The apparent absorbance, or optical density, of a solution can be used as an indicator of the level of light scattering caused by particles suspended in a solution. One

quality that this method can be used to examine is the concentration of particles suspended in solution.

The light scattering effects of particles suspended in liquid are determined by passing a beam of light of a known intensity and wavelength through the solution. The decrease in intensity of the light hitting a detector on the other side of the solution is used to determine how much light the particles in solution scattered (Figure 13).

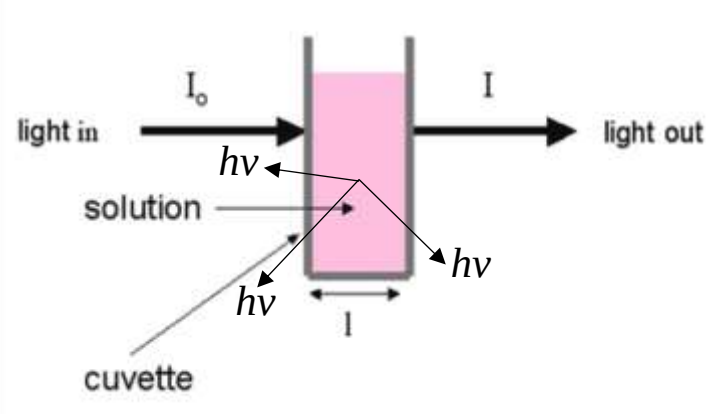

Figure 13. Model of light scattering during spectrophotometry. Spectroscopy can be used to analyze light scattering by cells in aqueous solution. When photons hit cells while passing through a solution some photons will scatter and some will make it through to the detector on the other side. Larger cells will typically scatter light more strongly than smaller cells.

Initial experiments in this direction focused on the light scattering effects of WT and *rad52* cells at the same concentration in solution. Both log and stationary phase cells were analyzed. Log phase WT cells displayed a 55.5% higher OD_{600} compared with stationary phase WT cells (compare Figure 14a, left column, vs 14b, left column). *rad52* cells in mid-log phase displayed a 66.1% higher OD_{600} than stationary phase *rad52* cells. It is likely that the log phase cells scatter light more strongly than the stationary phase

cells because they contain a much higher percentage of budded cells, which are larger than unbudded cells. Stationary phase *rad52* cells also exhibited higher light scattering than stationary phase WT cells, but the magnitude of the increase was not as great (Figure 14b). These results demonstrate that *rad52* cells scatter light more strongly than WT cells, regardless of growth phase. This is consistent with earlier results indicating *rad52* cells having larger average sizes in both log and stationary phases.

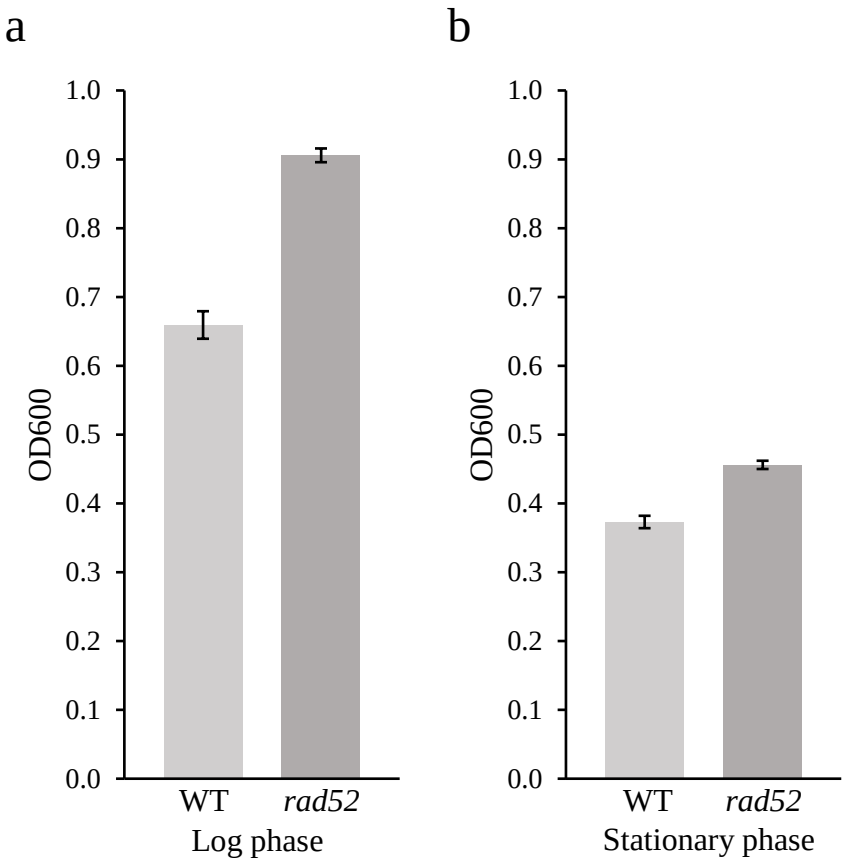

Figure 14. Light scattering by log and stationary phase WT and *rad52* cells. a) During log phase growth, *rad52* cells display a pronounced increase in optical density compared to WT cells. b) During stationary phase growth *rad52* cells still have a significantly higher OD_{600} than WT cells, but the difference between them is reduced. All cultures contained $1x10^7$ cells/mL and four replicates were analyzed. Averages and standard deviations are shown.

Cells suspended in solution will naturally sediment to the bottom of their container over time, barring physical agitation of the solution. Large cells typically sediment faster than smaller cells (Figure 15).

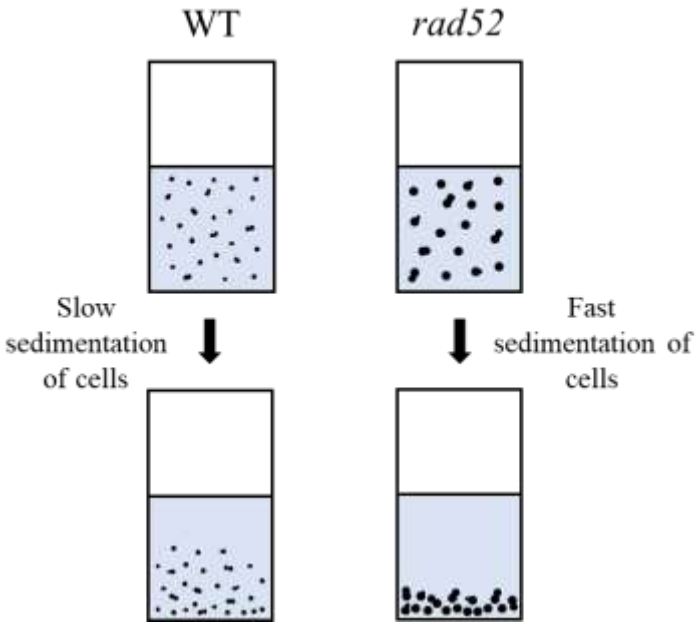

Figure 15. Model of rate of sedimentation differences between WT and *rad52* cells. *rad52* cells tend to be both larger and possess higher percentages of large-budded cells than their WT counterparts. It is possible that due to these factors *rad52* cells sediment out of solution faster than WT cells.

It was suspected that *rad52* cells, due to their higher percentage of large-budded cells and generally larger cell size, would sediment faster than WT cells. The rates of sedimentation of WT and *rad52* cells were examined. To accomplish this, OD_{600} measurements were taken at 10 minute intervals over a period of 70 minutes. Over time, solutions of WT and *rad52* cells displayed a decrease in OD_{600}. The decrease corresponded with cells sedimenting towards the bottom of the cuvette and out of the beam of light used for taking the measurements. The difference between the rate of

decrease of OD_{600} in WT and *rad52* cells was most obvious in log phase cells (Figure 16a). The faster rate of sedimentation of *rad52* cells is most likely due to the higher level of large-budded cells and in larger average sizes. As shown in Figure 16b, the log phase *rad52* cells had approximately 50% large-budded cells when analyzed in the microscope, while the WT cultures only contained approximately 28% large-budded cells. The difference between WT and *rad52* cells was less pronounced in stationary phase cultures (Figure 16c). This similarity may be due to the fact that both stationary phase cultures had approximately 90% unbudded G_1 cells and very few large-budded cells (Figure 16d).

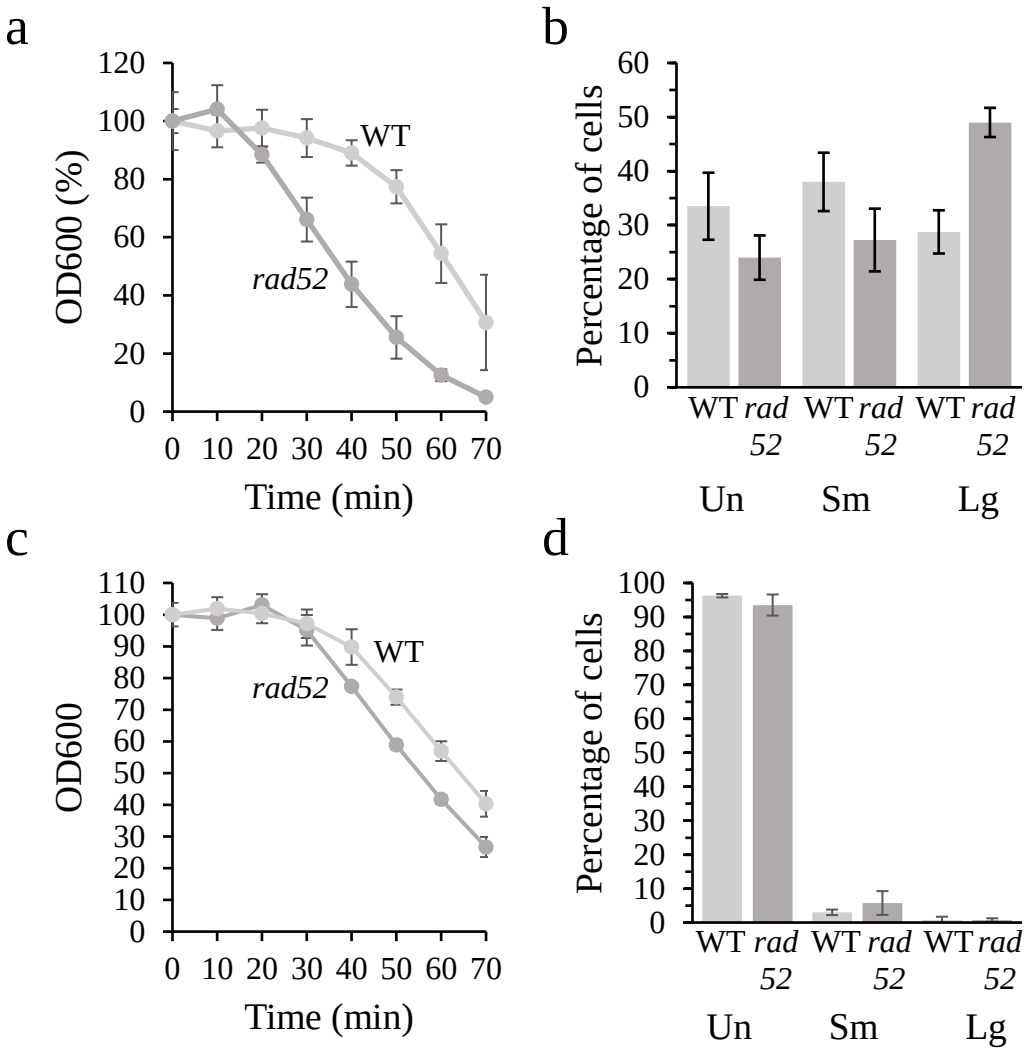

Figure 16. Sedimentation time courses and cell cycle phase distributions of log and stationary phase *S. cerevisiae* cells. a) Time-course experiment measuring OD_{600} of mid-log phase cells at 10 min intervals to determine rate of sedimentation. b) The percentage of unbudded (Un), small-budded (Sm), and large-budded (Lg) cells in the log phase culture at the 0 minute timepoint. c) Time-course experiment measuring OD_{600} of stationary phase cells at 10 minutes intervals to determine rates of sedimentation. d) The percentage of unbudded (Un), small-budded (Sm), and large-budded (Lg) cells in the stationary phase cultures at the 0 minute timepoint.

Evidence presented by Monica Weis indicated that the elevated large-budded cell levels in *rad52* cells is due to constitutive activation of the DNA damage checkpoint (44).

She determined this by creating seven double mutants combining *RAD52* inactivation with inactivation of genes vital for the activation of the DNA damage checkpoint. All seven double mutants displayed large-budded cell percentages similar to WT cells rather than *rad52* cells. To continue this type of genetic investigation, the recently described relationship between the *RAD52* gene and the spindle assembly checkpoint was analyzed (40).

The spindle assembly checkpoint occurs during mitosis after the DNA damage checkpoint. Its purpose is to ensure that the sister chromatids are attached properly to the mitotic spindle during metaphase and will be segregated correctly so that each daughter cell gets one copy. It has recently been suggested that Rad52 regulates the recruitment of the protein Mps1 to kinetochores, which is a vital step in the spindle assembly checkpoint (40). It is possible that some large-budded cells in *rad52* cultures might be M phase cells that have arrested at the spindle assembly checkpoint. Due to the role played by Mad1 and Mad2 in the spindle assembly checkpoint, the effects of their deletion on large-budded cell levels in *rad52* mutants was examined by creating *mad1* and *mad2* single mutants and double mutants of the same and *rad52*.

The process of creating these, and other, knockout mutants is explained in brief in Figure 17a. A *LEU2* gene-containing DNA fragment was created to perform the gene knockout. Both ends of this fragment had sequences homologous to the gene that was to be knocked out, *RAD52*. Once the DNA fragment was transformed into yeast cells, HR can replace the *RAD52* gene targeted for knockout with the inserted fragment due to genetic exchange between the end homologous sequences. Chromosomal DNA was extracted from independent Leu^+ transformants and used to carry out PCR confirmation

tests. Primers were selected so that one would have homology to the inserted *LEU2* sequence (Leu2A primer) and the other would have homology to part of the chromosome upstream of the inactivated *RAD52* gene (Figure 17b). The purpose of this was to ensure that the fragment had been inserted in the desired place and the targeted *RAD52* gene had indeed been knocked out.

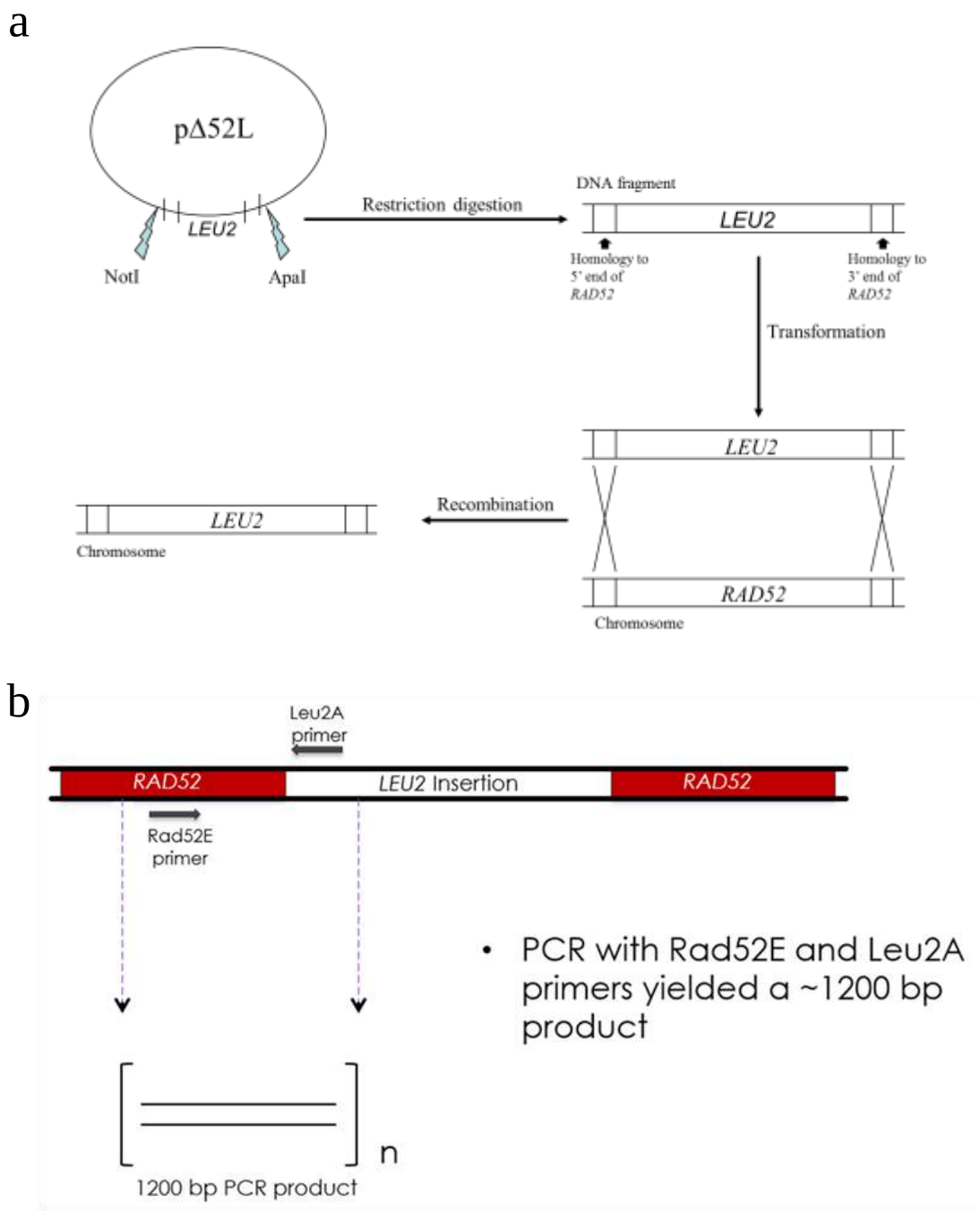

Figure 17. The creation and confirmation of a knockout mutant. a) An explanation of the gene knockout procedure displaying the replacement of *RAD52* with the selectable marker *LEU2*. b) The method by which a gene knockout of *RAD52* with *LEU2* was confirmed.

Knowledge of the sequences of the primers, the *LEU2* gene, and the area neighboring the *RAD52* knockout region allowed for the detection of the product

fragment. An aliquot of each PCR reaction was run on an agarose gel. Figure 18 below is an agarose gel run to confirm the correct knockout of *RAD52* and insertion of *LEU2*. Bands of 1200 bp were seen for each isolate tested, confirming the successful knockout (Figures 8).

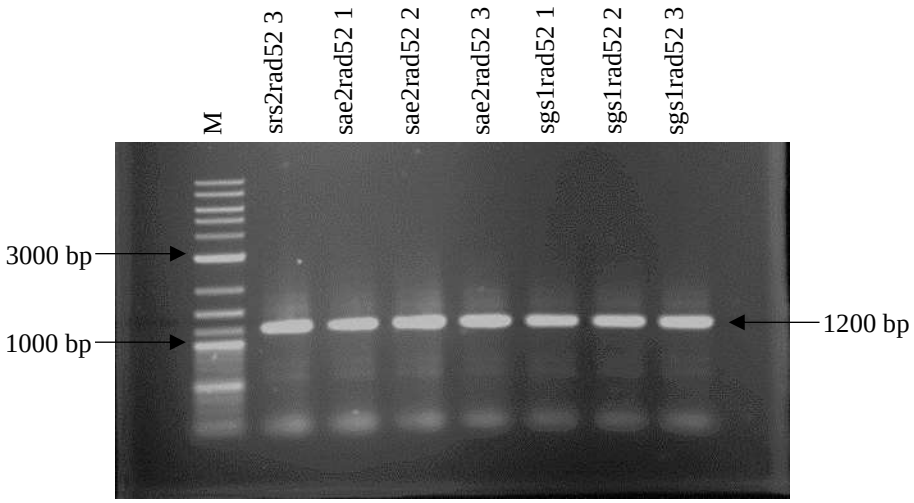

Figure 18. Example of a PCR confirmation experiment performed to identify clones with *LEU2* inserted into *RAD52*. The lanes in this 0.8% agarose gel contained, from left to right, PCR products from *srs2 rad52*, *sae2 rad52*, and *sgs1 rad52* transformations which I created. In each of these lanes the expected 1200 bp band for a *rad52Δ::LEU2* insertion was detected. The faint, bottom band represents unused primers. The lane represented by M contains a 2-log DNA ladder.

After creation and PCR confirmation of new *mad1 rad52* and *mad2 rad52* double mutants, the strains were grown to log phase and levels of large-budded G_2/M cells were measured. WT and *rad52* cells were also included as control. The *rad52*, *mad1*, and *mad2* single mutants all had large-budded percentages near 55%, which is approximately 20% above that of WT cells (Figure 9 and Figure 19). The mean large-budded cell percentages of the *rad52 mad1* and *rad52 mad2* double mutants were even higher, at

approximately 35% above WT cells. This suggests that the effects of combining deletions of *RAD52* with *MAD1* or *MAD2* are additive, implying that each contributes on their own to the levels of large-budded cells. In other words, the cause of large-budded cells in *rad52* cells (likely DSBs) is different from the cause of large-budded cells in *mad1* or *mad2* mutants.

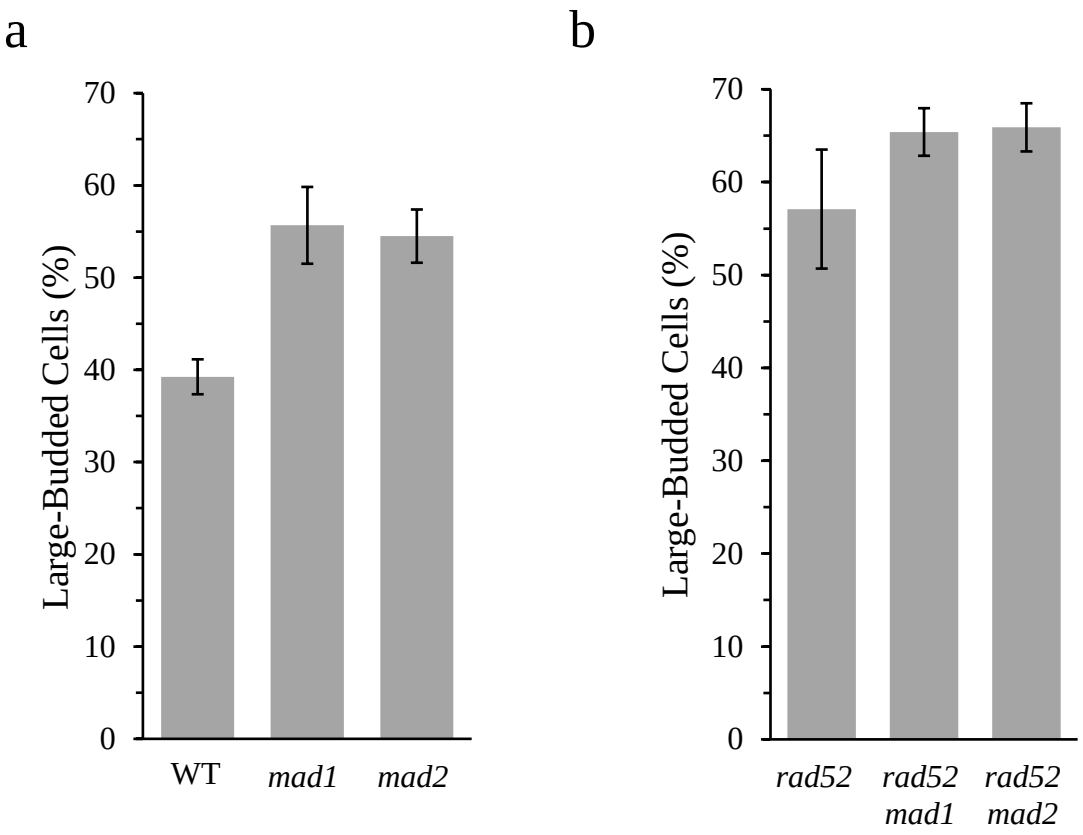

Figure 19. Levels of large-budded cells in log phase cultures of *rad52* and *mad1* or *mad2* single and double mutants. a) Large-budded cell percentages in *mad1* and *mad2* single mutants. b) Large-budded cell percentages in *rad52*, *rad52 mad1*, and *rad52 mad2* cells.

Several genes play a role in the initial steps of the HR pathway, before genetic exchange occurs and before the DNA damage checkpoint is initiated (Figure 20). The DSB ends are initially resected by Sae2 and the Mrx complex to form short ssDNA tails.

This is followed by more resection by Exo1 and the Sgs1-Dna2 complex to produce much larger ssDNA tails. After resection, the ssDNA binding protein Rpa binds to the ssDNA tails and signals the recruitment of Rad51 and Rad52 to the location of the break (Figure 20). Rpa also recruits Mec1-Ddc2, which activates the DNA damage checkpoint response.

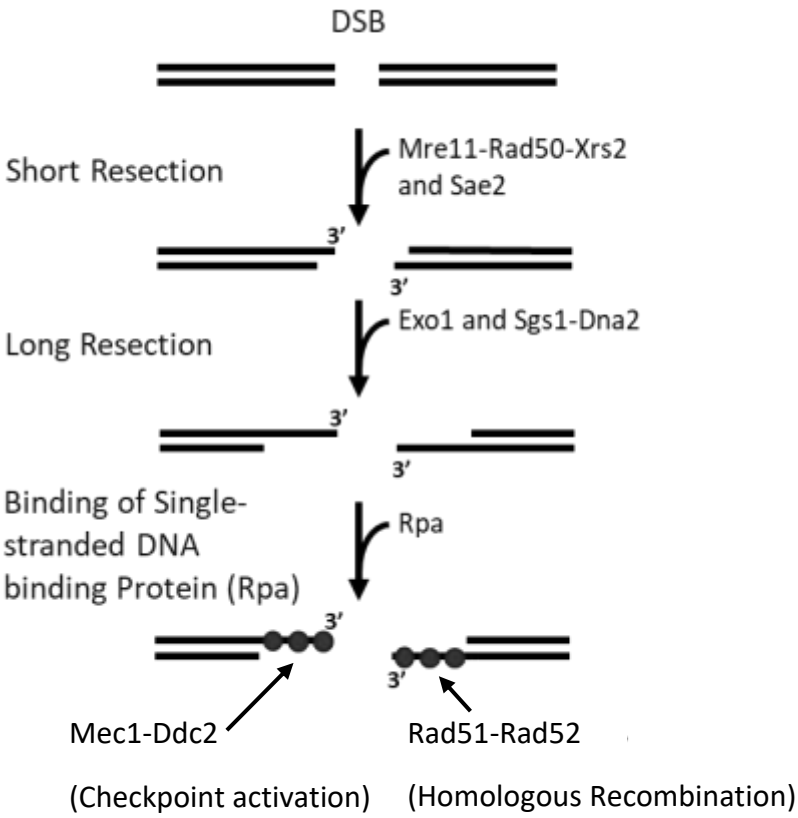

Figure 20. The initial resection and binding steps of the HR pathway. These steps allow for the recruitment of Rad51 and Rad52 to complete HR and Mec1-Ddc2 to initiate the DNA damage checkpoint response.

Spontaneously occurring DSBs in *rad52* cells do not get repaired efficiently. It is likely that the DSB ends do get processed by the HR pathway nucleases to eventually form Rpa-coated ssDNA tails that then recruit Mec1-Ddc2. These proteins then initiate a

checkpoint response that causes the cells to pause in G_2 phase to try to allow more time for repair of the DSBs before going into M phase. If this model is correct, then reducing resection should lead to less Rpa-coated ssDNA and a smaller checkpoint activation signal, which would also result in fewer G_2 phase-arrested cells in a *rad52* cell culture. This idea was tested by inactivating resection nuclease genes to create *sae2 rad52*, *exo1 rad52*, and *srs2 rad52* double mutants.

To investigate the importance of the short resectioning step, *sae2 rad52* double mutants were created. They were chosen instead of *mrx rad52* due to a lower impact on cell viability than a double mutant lacking a component of the Mrx complex. Initial testing made use of a Lewis lab *sae2Δ::HygB*^{r} *rad52Δ::URA3* strain that had been created years ago. The level of large-budded cells during log phase seen in these *rad52 sae2* cells was near that of *rad52* cells and much higher than WT levels (Figure 21a). In order to assess *sae2*'s role another way, *rad52Δ::LEU2 sae2Δ::G418*^{r} double mutants were created for this study. The level of large-budded cells seen with this *sae2 rad52* double mutant was also near that of *rad52* single mutants (Figure 21b).

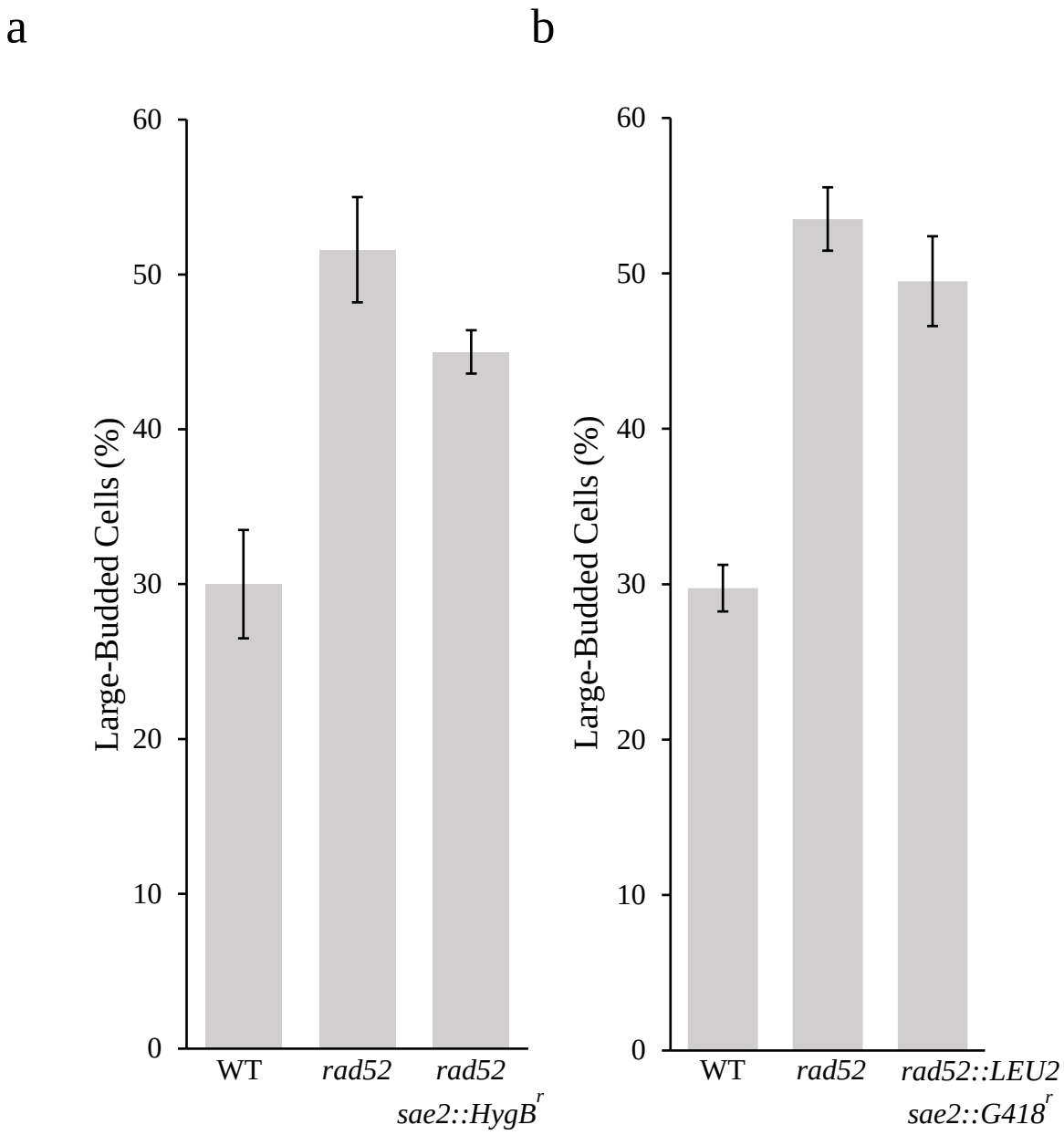

Figure 21. Levels of large-budded G_2/M in nuclease-defective *sae2 rad52* double mutants. a) *rad52Δ::URA3 sae2Δ::HygB*^{r} cells. b) *rad52Δ::Leu2 sae2Δ::G418*^{r} cells.

The long resectioning step was investigated in similar ways. Initially, yeast deletion library-derived *exo1* and *exo1 rad52* strains were tested. The double mutant was created by inactivating *RAD52* in an *exo1* single mutant obtained from a collection of yeast deletion library strains. It was seen that during log phase growth the level of large-budded cells in the *exo1 rad52* double mutants remained high, near that of *rad52* single

mutants (Figure 22a). To confirm these results I created and tested new *rad52Δ::LEU2 exo1Δ::G418*^{r} double mutants that did not originate from a yeast deletion strain library. I inactivated *EXO1* and then inactivated *RAD52*, confirming each gene knockout by PCR as before. Two independent isolates were selected for testing. Each double mutant had elevated levels of large-budded cells during log phase growth that closely corresponded with *rad52* levels (Figure 22b). This result is in accord with the outcome seen in the library strain derived *exo1 rad52* strain (Figure 22a).

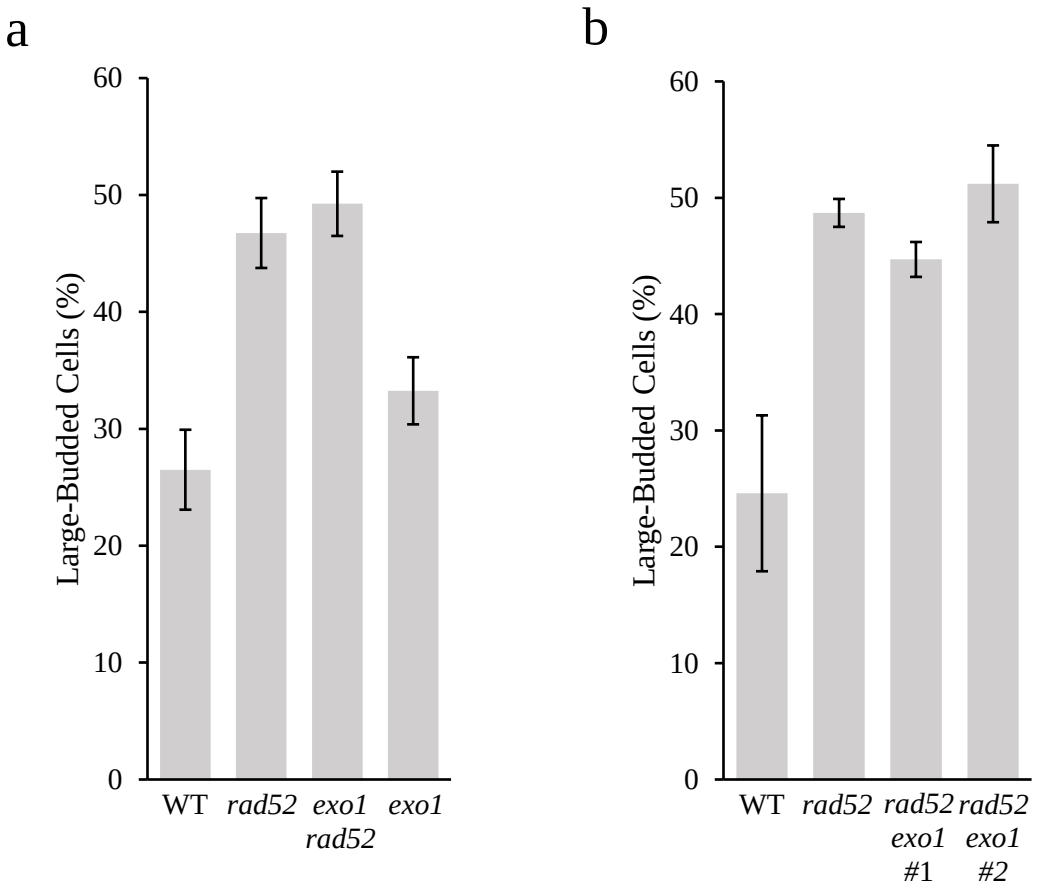

Figure 22. Levels of large-budded G_2/M in nuclease-defective *exo1 rad52* double mutants. a) Library-derived strains of *exo1* and *exo1 rad52*. b) *rad52 exo1* double mutants made from BY4741.

The long resectioning step was also investigated using *sgs1 rad52* double mutants. Initial results with *MATα* library-derived strains were exciting and suggested that loss of *SGS1* in a *rad52* mutant would return the level of large-budded cells to WT levels (Figure 23a). These double mutants were created by inactivating *RAD52* in a *MATα* library *sgs1* mutant. However, when opposite mating type *MATa* library strains of these mutants were created and tested, the level of large-budded cells exhibited by *sgs1 rad52* cells remained high, at *rad52* levels (Figure 23b). To clarify these results, fresh *MATα sgs1 rad52* double mutants were created by knocking out *SGS1* and then knocking out *RAD52* in WT BY4742 cells. The level of large-budded cells seen in these new double mutants was also high, corresponding closely with *rad52* single mutant levels (Figure 23c). There may be an unknown gene mutation inside the *MATα sgs1* library strain used to create *sgs1 rad52* double mutants for the experiments shown in Figure 23a that caused the results to be different. The results shown in Figure 23b and 23c indicate that the loss of Sgs1-Dna2 nuclease activity does not reduce the constitutively activated checkpoint signal in *rad52* cells.

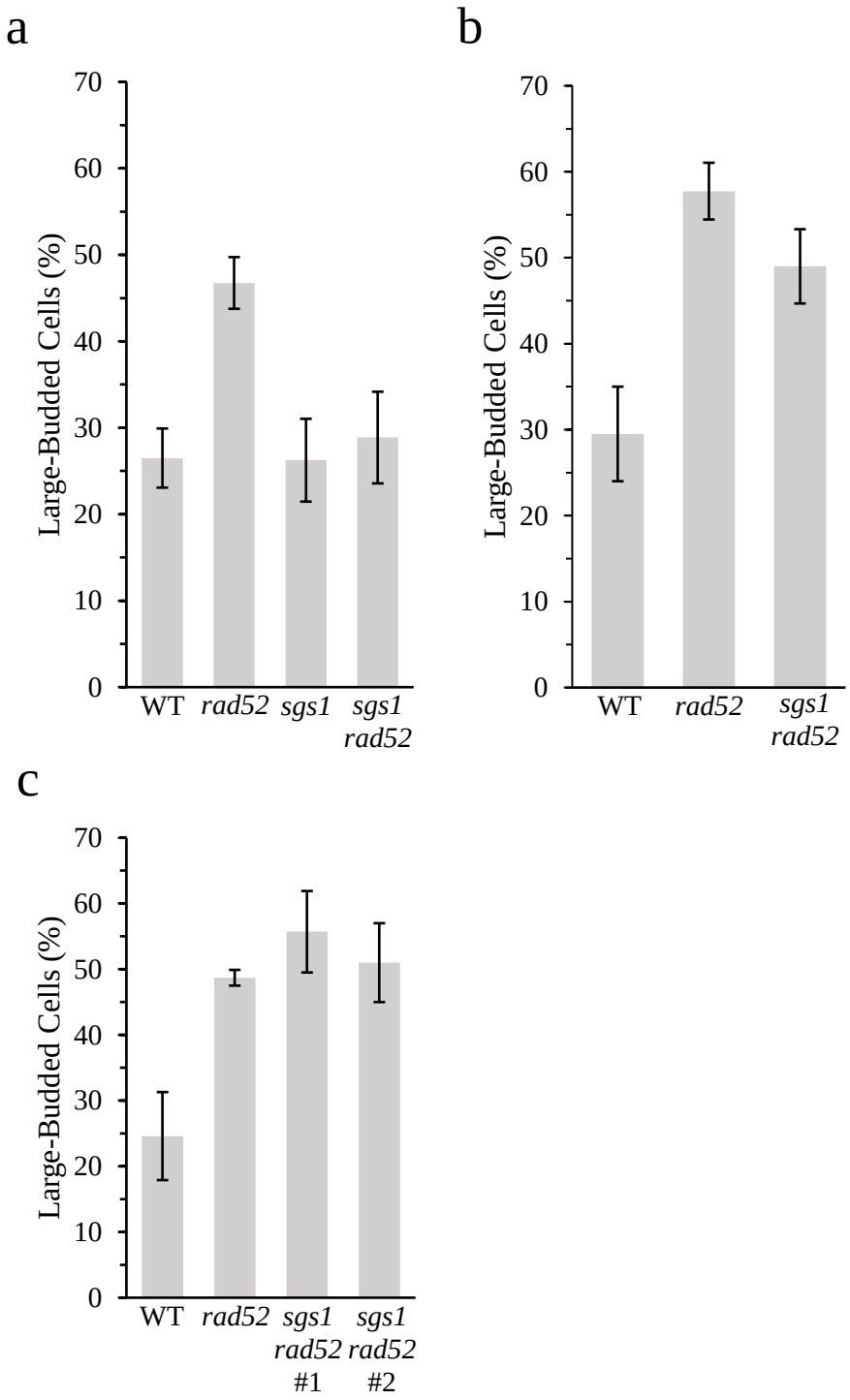

Figure 23. Levels of large-budded G_2/M in helicase-defective *sgs1 rad52* double mutants. a) *MATα* library-derived *sgs1 rad52* cells. b) *MATa* library-derived *sgs1 rad52* cells. c) New *MATα rad52 sgs1* cells not derived from a yeast deletion library strain collection.

Sgs1 is thought to form a complex with Rmi1 and Top3 that plays a role in rescue of arrested replication forks and possibly in resectioning of DSB ends (Figure 24a). To test the impact of removing Rmi1 or Top3, *rmi1 rad52* and *top3 rad52* double mutants were created and examined. During log phase growth, the level of large-budded cells in the *rmi1 rad52* and *top3 rad52* double mutants was high, close to or even higher than the levels seen in *rad52* cells (Figure 24b).

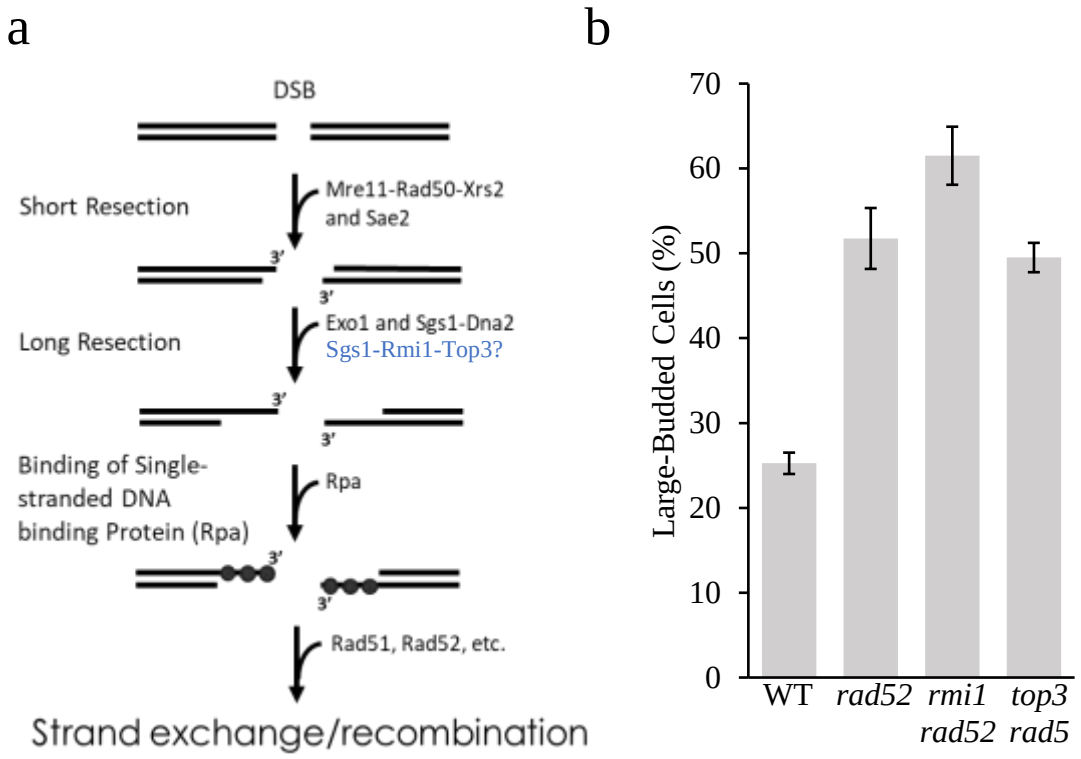

Figure 24. Roles of Rmi1 and Top3 in HR and effects of their loss in *rad52* mutants. a) Diagram indicating possible role of Rmi1 and Top3 in DSB end resection. b) Fraction of large-budded cells in *rad52 rmi1* and *rad52 top3* double mutants.

Oxygen-derived free radicals can cause oxidative stress in cells, leading directly or indirectly to DNA DSBs. The presence of DSBs in a cell can lead to the activation of the DNA damage checkpoint, which can prolong the amount of time spent by a cell in G_2 phase. Therefore, it is reasonable to suggest that oxidative stress could be a factor in the elevated levels of large-budded cells seen in *rad52* mutants given their reduced ability to carry out HR. If reactive oxygen species (ROS) are major sources of the DSBs in *rad52* cells, then adding radical quenching antioxidants to the cells might reduce DSBs and therefore decrease the strong G_2 phase arrest response. To test this idea, experiments were carried out using various concentrations of the strong antioxidant N-acetylcysteine (NAC) mixed into YPDA plates and liquid cultures. WT and *rad52* cells were incubated on YPDA plates containing 50 mM NAC and then grown to mid-log phase in YPDA liquid broth containing the same concentration of NAC. Cells were also grown on media without NAC. For both WT and *rad52* cells a trend toward lower large-budded percentages were seen, but the standard deviations between the treated and control cultures were overlapping (Figure 25). Experiments were also run with concentrations of NAC at and above 100 mM, but the growth of cells was negatively impacted.

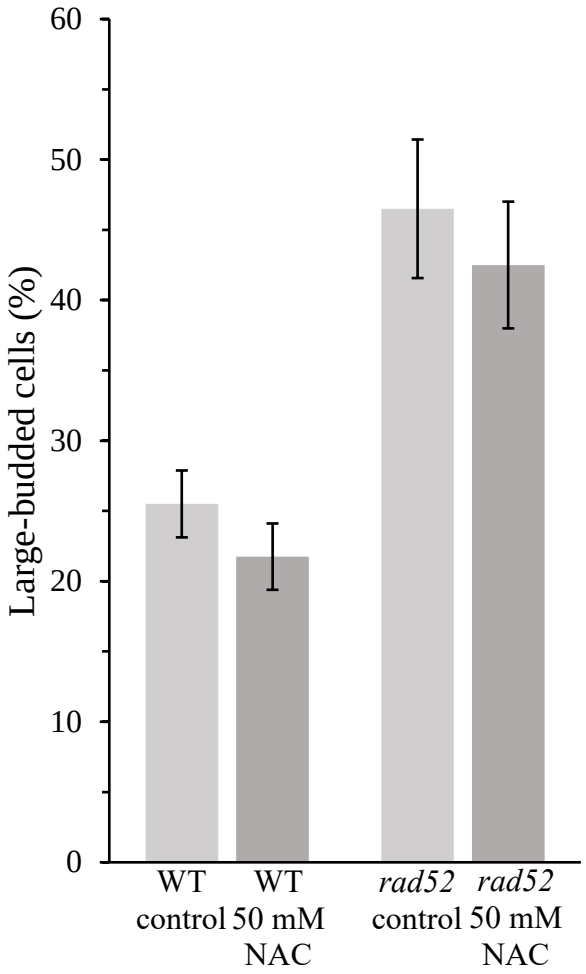

Figure 25. Percentage of large-budded cells in WT and *rad52* cell cultures grown to log phase in the presence or absence of NAC.

Inspired by the work of Kwolek-Mirek *et al.*, the efficacy of a cocktail of 5 mM NAC, cysteine (CYS), reduced glutathione (GSH), and ascorbate (ASC) (vitamin C) for reducing the percentage of large-budded cells in mid-log phase *rad52* cells was tested. As in the previous experiment, cells were incubated on YPDA plates containing the cocktail at the mentioned concentration and then harvested and grown to mid-log phase in YPDA liquid broth which also contained the cocktail. No significant change was seen in *rad52* cells grown with the cocktail compared to *rad52* cells grown without (Figure 26).

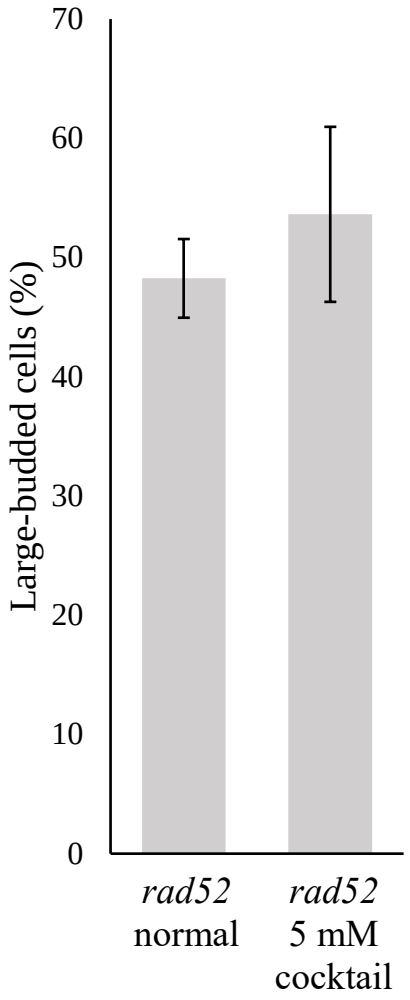

Figure 26. Comparison of *MATα rad52* cells grown in pure YPDA against those grown in YPDA with 5 mM NAC, CYS, GSH, and ASC. The cocktail failed to reduce the level of large-budded cells in mid-log *rad52* cultures.

A number of *S. cerevisiae* strains were provided to us by Dr. Cory Holland that have Green Fluorescent Protein (GFP) fused with various proteins involved in the response to DNA DSBs. These cells can potentially be used with fluorescence or contrast microscopy to physically observe concentrations of the fused proteins in response to DNA damaging events, such as treatment with methyl methanesulfonate (MMS**)** (24). In anticipation of future experiments, I created *rad52* knockout mutants of Ddc2::GFP and Rfa1::GFP strain (Table 1). The knockouts were confirmed with PCR (Figure 27).

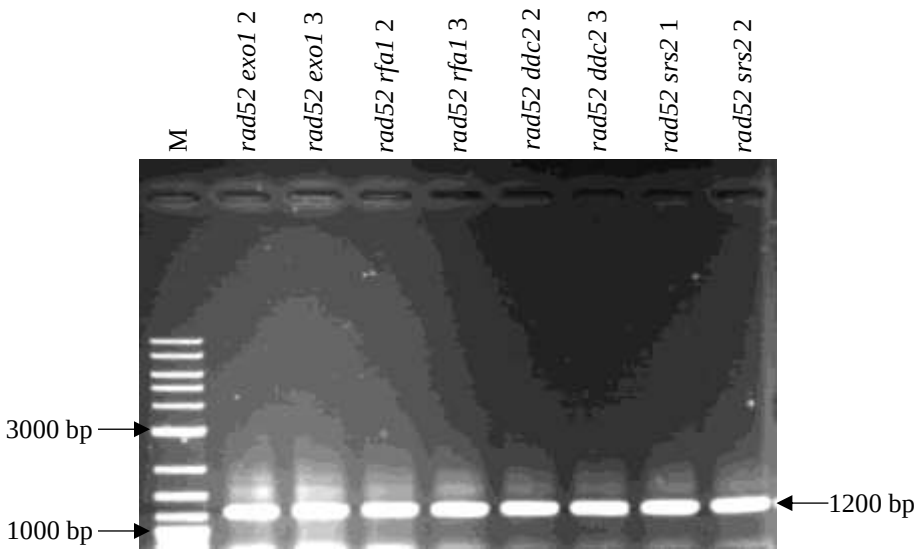

Figure 27. PCR confirmation of insertion of *LEU2* into *RAD52* in strains containing RFA1::GFP and DDC2::GFP fusions on a 0.8% agarose gel (lanes 4, 5, and 6 from left to right). RAD52E and Leu2A primers were used as described previously. The second and third lane represent confirmation of *rad52 exo1* mutants and the eighth and ninth lanes represent the confirmation of *rad52 srs2* mutants. The presence of a 1.2 kb band is an indication of a successful *LEU2* gene insertion. The lane represented by M contains a 2-log DNA ladder.

IV. SUMMARY AND CONCLUSIONS

Work by previous graduate student Monica Weis demonstrated that an unusually high level of large-budded G_2 cells are present in *rad52* cell cultures. By abolishing this elevated level through the creation of several *rad52* mutants that also had DNA damage checkpoint response gene knockouts, she provided evidence that the elevated level of large-budded cells was due to activation of the DNA damage checkpoint. The phenomenon is most likely due to unrepaired, naturally occurring DNA DSBs that are inefficiently repaired in the HR-deficient *rad52* cells. My experiments with *rad51* cells confirmed that these HR-deficient mutants have characteristics similar to *rad52* cells, such as elevated large-budded cell levels and slow doubling times. However, this work revealed that the phenotypes were much more extreme in *rad52* cells than in *rad51* mutants. This is consistent with past studies showing that Rad52 is much more critical then Rad51 in many assays of HR (25, 27, 51).

Monica Weis examined the sizes of unbudded and budded WT and *rad52* cells during log phase growth. I furthered this work by examining the sizes of unbudded and budded WT and *rad52* cells during stationary phase. I observed that the trends seen during log phase growth are mostly conserved in stationary phase cells, with *rad52* cells having consistently larger average sizes than WT cells.

Aberrant cells with more than one bud are sometimes seen while working with *S. cerevisiae* cells and appeared to be more common in *rad52* cells than in WT cells. To this end I counted multibudded cells in both *MATa* and *MATα* WT and *rad52* log phase cultures. In both mating types, *rad52* mutant cultures had elevated levels of multibudded

cells compared to WT cell cultures indicating that the loss of *RAD52* may destabilize cell cycle timing.

We made use of FACS analysis and a DNA staining fluorophore to analyze the relative levels of cells with 1n versus 2n DNA content inside log phase WT and *rad52* cell cultures. *MATa* and *MATα rad52* mutants displayed a strongly increased level of cells with G_2/M DNA content when compared with WT cell cultures, which was consistent with the phase contrast microscopy findings.

Several physical properties of *rad52* cells were examined with spectrophotometry. At equal cell titers ($1x10^7$ cells/mL) aqueous solutions of *rad52* cells displayed more light scattering than solutions containing WT cells. Sedimentation experiments revealed that stationary phase WT and *rad52* cells sediment out of solution over a similar amount of time. However, log phase *rad52* cells sediment at a much higher rate than WT cells. This is most likely due to the increase in the number of budded cells, especially large-budded cells, in log-phase *rad52* cultures. The electrical conductivity of WT and *rad52* cells was tested, but no great difference was seen in their values.

Several double mutants were created to test the role of resectioning steps in generation of a DNA damage checkpoint signal in *rad52* cells. The exonucleases Sae2 and Exo1, as well as the helicase Sgs1, play a role in end resection at sites of DSBs. Double mutants, lacking both *RAD52* and a resection nuclease gene, were examined during log phase growth to determine percentages of large-budded cells. Knockout of *SAE2*, *SGS1*, or *EXO1* in a *rad52* mutant failed to restore levels of large-budded cells to WT levels. Rmi1 and Top3 interact with Sgs1 to rescue replication forks and possibly to perform DSB end resection as well (32). As before, *top3 rad52* and *rmi1 top3* double

mutants did not show significantly reduced levels of large-budded cells. It is possible that the loss of any one of these nucleases in a cell can be compensated by the presence of other nucleases. In future studies, additional mutants should be tested that have two or more of the nucleases inactivated to test this new idea.

DSBs inside living cells can be caused either directly or indirectly by ROS. Given that the presence of DSBs inside a living cell is a likely trigger for the G_2/M DNA damage checkpoint, the effects of adding antioxidants to growth media were examined. Addition of NAC or a cocktail of NAC plus three other antioxidants failed to reduce the level of large-budded cells in *rad52* mutants. Higher concentrations of antioxidants were also tested, but they led to impaired growth of the cells that prevented the collection of any useful results. It is possible that higher levels of antioxidants than could be achieved in these experiments are required to produce an effect. Future work should test alternative approaches, such as manipulation of cellular levels of antioxidant enzymes.

REFERENCES

1. Hoeijmakers, J. H., DNA damage, aging, and cancer. *N Engl J Med* 2009, *361* (15), 1475-85.

2. Ames, B. N.; Shigenaga, M. K.; Hagen, T. M., Oxidants, antioxidants, and the degenerative diseases of aging. *Proceedings of the National Academy of Sciences of the United States of America* 1993, *90* (17), 7915-22.

3. Hubscher, U.; Maga, G., DNA replication and repair bypass machines. *Curr Opin Chem Biol* 2011, *15* (5), 627-35.

4. De Bont, R.; van Larebeke, N., Endogenous DNA damage in humans: a review of quantitative data. *Mutagenesis* 2004, *19* (3), 169-85.

5. Finn, K.; Lowndes, N. F.; Grenon, M., Eukaryotic DNA damage checkpoint activation in response to double-strand breaks. *Cell Mol Life Sci* 2012, *69* (9), 1447-73.

6. Ramey, C. J.; Howar, S.; Adkins, M.; Linger, J.; Spicer, J.; Tyler, J. K., Activation of the DNA damage checkpoint in yeast lacking the histone chaperone anti-silencing function 1. *Mol Cell Biol* 2004, *24* (23), 10313-27.

7. Felske, L. R.; Lenz, S. A. P.; Wetmore, S. D., Quantum Chemical Studies of the Structure and Stability of N-Methylated DNA Nucleobase Dimers: Insights into the Mutagenic Base Pairing of Damaged DNA. *The journal of physical chemistry. A* 2017.

8. Ciccia, A.; Elledge, S. J., The DNA damage response: making it safe to play with knives. *Molecular cell* 2010, *40* (2), 179-204.

9. Schmidt, K. H.; Kolodner, R. D., Requirement of Rrm3 helicase for repair of spontaneous DNA lesions in cells lacking Srs2 or Sgs1 helicase. *Mol Cell Biol* 2004, *24* (8), 3213-26.

10. Bhattacharjee, S.; Nandi, S., Rare Genetic Diseases with Defects in DNA Repair: Opportunities and Challenges in Orphan Drug Development for Targeted Cancer Therapy. *Cancers (Basel)* 2018, *10* (9).

11. Ragu, S.; Faye, G.; Iraqui, I.; Masurel-Heneman, A.; Kolodner, R. D.; Huang, M. E., Oxygen metabolism and reactive oxygen species cause chromosomal rearrangements and cell death. *Proceedings of the National Academy of Sciences of the United States of America* 2007, *104* (23), 9747-52.

12. Swenberg, J. A.; Lu, K.; Moeller, B. C.; Gao, L.; Upton, P. B.; Nakamura, J.; Starr, T. B., Endogenous versus exogenous DNA adducts: their role in carcinogenesis, epidemiology, and risk assessment. *Toxicol Sci* 2011, *120 Suppl 1*, S130-45.

13. Neddermann, P.; Gallinari, P.; Lettieri, T.; Schmid, D.; Truong, O.; Hsuan, J. J.; Wiebauer, K.; Jiricny, J., Cloning and expression of human G/T mismatch-specific thymine-DNA glycosylase. *J Biol Chem* 1996, *271* (22), 12767-74.

14. Cavalieri, E.; Saeed, M.; Zahid, M.; Cassada, D.; Snow, D.; Miljkovic, M.; Rogan, E., Mechanism of DNA depurination by carcinogens in relation to cancer initiation. *IUBMB Life* 2012, *64* (2), 169-79.

15. Buis, J. M.; Cheek, J.; Kalliri, E.; Broderick, J. B., Characterization of an active spore photoproduct lyase, a DNA repair enzyme in the radical S-adenosylmethionine superfamily. *J Biol Chem* 2006, *281* (36), 25994-6003.

16. Lisby, M.; Mortensen, U. H.; Rothstein, R., Colocalization of multiple DNA double-strand breaks at a single Rad52 repair centre. *Nat Cell Biol* 2003, *5* (6), 572-7.

17. Obe, G.; Johannes, C.; Schulte-Frohlinde, D., DNA double-strand breaks induced by sparsely ionizing radiation and endonucleases as critical lesions for cell death, chromosomal aberrations, mutations and oncogenic transformation. *Mutagenesis* 1992, *7* (1), 3-12.

18. Bauer, N. C.; Corbett, A. H.; Doetsch, P. W., The current state of eukaryotic DNA base damage and repair. *Nucleic Acids Res* 2015, *43* (21), 10083-101.

19. Wallace, S. S., Base excision repair: a critical player in many games. *DNA Repair (Amst)* 2014, *19*, 14-26.

20. Spivak, G., Nucleotide excision repair in humans. *DNA Repair (Amst)* 2015, *36*, 13-8.

21. Pannunzio, N. R.; Watanabe, G.; Lieber, M. R., Nonhomologous DNA end-joining for repair of DNA double-strand breaks. *J Biol Chem* 2018, *293* (27), 10512-10523.

22. Emerson, C. H.; Bertuch, A. A., Consider the workhorse: Nonhomologous end-joining in budding yeast. *Biochem Cell Biol* 2016, *94* (5), 396-406.

23. Lewis, L. K.; Resnick, M. A., Tying up loose ends: nonhomologous end-joining in Saccharomyces cerevisiae. *Mutation research* 2000, *451* (1-2), 71-89.

24. Lisby, M.; Rothstein, R., Choreography of recombination proteins during the DNA damage response. *DNA Repair (Amst)* 2009, *8* (9), 1068-76.

25. Kowalczykowski, S. C., An Overview of the Molecular Mechanisms of Recombinational DNA Repair. *Cold Spring Harb Perspect Biol* 2015, *7* (11).

26. Jones, R. E.; Humphrey, T. C., Chapter 8 - Homologous Recombination and Nonhomologous End-Joining Repair in Yeast A2 - Kovalchuk, Igor. In *Genome Stability*, Kovalchuk, O., Ed. Academic Press: Boston, 2016; pp 117-135.

27. Game, J. C., The Saccharomyces repair genes at the end of the century. *Mutation research* 2000, *451* (1-2), 277-93.

28. McKinney, J. S.; Sethi, S.; Tripp, J. D.; Nguyen, T. N.; Sanderson, B. A.; Westmoreland, J. W.; Resnick, M. A.; Lewis, L. K., A multistep genomic screen identifies new genes required for repair of DNA double-strand breaks in Saccharomyces cerevisiae. *BMC Genomics* 2013, *14*, 251.

29. Yin, Y.; Petes, T. D., The role of Exo1p exonuclease in DNA end resection to generate gene conversion tracts in Saccharomyces cerevisiae. *Genetics* 2014, *197* (4), 1097-109.

30. Cejka, P., DNA End Resection: Nucleases Team Up with the Right Partners to Initiate Homologous Recombination. *J Biol Chem* 2015, *290* (38), 22931-8.

31. Niu, H.; Chung, W. H.; Zhu, Z.; Kwon, Y.; Zhao, W.; Chi, P.; Prakash, R.; Seong, C.; Liu, D.; Lu, L.; Ira, G.; Sung, P., Mechanism of the ATP-dependent DNA end-resection machinery from Saccharomyces cerevisiae. *Nature* 2010, *467* (7311), 108-11.

32. Hickson, I. D.; Mankouri, H. W., Processing of homologous recombination repair intermediates by the Sgs1-Top3-Rmi1 and Mus81-Mms4 complexes. *Cell Cycle* 2011, *10* (18), 3078-85.

33. Dodson, G. E.; Shi, Y.; Tibbetts, R. S., DNA replication defects, spontaneous DNA damage, and ATM-dependent checkpoint activation in replication protein A-deficient cells. *J Biol Chem* 2004, *279* (32), 34010-4.

34. Weinert, T. A.; Hartwell, L. H., The RAD9 gene controls the cell cycle response to DNA damage in Saccharomyces cerevisiae. *Science* 1988, *241* (4863), 317-22.

35. Alvaro, D.; Lisby, M.; Rothstein, R., Genome-wide analysis of Rad52 foci reveals diverse mechanisms impacting recombination. *PLoS Genet* 2007, *3* (12), e228.

36. Jorgensen, P.; Nishikawa, J. L.; Breitkreutz, B.-J.; Tyers, M., Systematic Identification of Pathways That Couple Cell Growth and Division in Yeast. *Science* 2002, *297*, 395-400.

37. Lewis, L. K.; Kirchner, J. M.; Resnick, M. A., Requirement for end-joining and checkpoint functions, but not RAD52-mediated recombination, after EcoRI endonuclease cleavage of Saccharomyces cerevisiae DNA. *Mol Cell Biol* 1998, *18* (4), 1891-902.

38. Tsong, A. E.; Tuch, B. B.; Johnson, A. D., CHAPTER 5: Rewiring Transcriptional Circuitry: Mating-Type Regulation in Saccharomyces cerevisiae and Candida albicans as a Model for Evolution. *Sex in Fungi* 2007, 76.

39. Klein, H. L., RDH54, a RAD54 homologue in Saccharomyces cerevisiae, is required for mitotic diploid-specific recombination and repair and for meiosis. *Genetics* 1997, *147* (4), 1533-43.

40. Lim, G.; Huh, W. K., Rad52 phosphorylation by Ipl1 and Mps1 contributes to Mps1 kinetochore localization and spindle assembly checkpoint regulation. *Proceedings of the National Academy of Sciences of the United States of America* 2017, *114* (44), E9261-E9270.

41. Rosen, G. M.; Pou, S.; Ramos, C. L.; Cohen, M. S.; Britigan, B. E., Free radicals and phagocytic cells. *FASEB J* 1995, *9* (2), 200-9.

42. Flora, S. J., Structural, chemical and biological aspects of antioxidants for strategies against metal and metalloid exposure. *Oxid Med Cell Longev* 2009, *2* (4), 191-206.

43. Kwolek-Mirek, M.; Zadrag-Tecza, R.; Bartosz, G., Ascorbate and thiol antioxidants abolish sensitivity of yeast Saccharomyces cerevisiae to disulfiram. *Cell Biology and Toxicology* 2012, *28* (1), 1-9.

44. Weis, M. F. DNA DOUBLE-STRAND BREAK REPAIR DEFICIENCY IS ASSOCIATED WITH CHANGES IN CELL CYCLING AND CELL MORPHOLOGY IN *SACCHAROMYCES CEREVISIAE*. Texas State University, 2017.

45. Brachmann, C. B.; Davies, A.; Cost, G. J.; Caputo, E.; Li, J.; Hieter, P.; Boeke, J. D., Designer deletion strains derived from Saccharomyces cerevisiae S288C: a useful set of strains and plasmids for PCR-mediated gene disruption and other applications. *Yeast* 1998, *14* (2), 115-32.

46. Sherman, F., Getting started with yeast. *Methods Enzymol* 2002, *350*, 3-41.

47. Lee, C. K.; Araki, N.; Sowersby, D. S.; Lewis, L. K., Factors affecting chemical-based purification of DNA from Saccharomyces cerevisiae. *Yeast* 2012, *29* (2), 73-80.

48. Tripp, J. D.; Lilley, J. L.; Wood, W. N.; Lewis, L. K., Enhancement of plasmid DNA transformation efficiencies in early stationary-phase yeast cell cultures. *Yeast* 2013, *30* (5), 191-200.

49. Looke, M.; Kristjuhan, K.; Kristjuhan, A., Extraction of genomic DNA from yeasts for PCR-based applications. *Biotechniques* 2011, *50* (5), 325-8.

50. Lanier, L. L., Just the FACS. *J Immunol* 2014, *193* (5), 2043-4.

51. Bartsch, S.; Kang, L. E.; Symington, L. S., RAD51 is required for the repair of plasmid double-stranded DNA gaps from either plasmid or chromosomal templates. *Mol Cell Biol* 2000, *20* (4), 1194-205.